BAMBOO

Project acronym:	BAMBOO
Title:	Biodiversity and trade: mitigating the impacts of non-food biomass global supply chains
Grant agreement number:	101059379

DELIVERABLE 1.1

Characterization factor model for ocean acidification (updated version after publication of paper)

Lead party for deliverable:	NTNU
Document type:	Report
Due date of deliverable:	31-10-2024
Actual submission date:	31-10-2024
Actual re-submission date	20-10-2025
Version:	2.0
Dissemination level:	Public
Authors:	Sedona Anderson, Francesca Verones, Konstantin Stadler (NTNU)
Reviewers:	Laura Scherer (ULEI); Stephan Pfister (ETH)

This project is funded by the European Union's Horizon Europe research and innovation programme under grant agreement no. 101059379.

Project funded by

Schweizerische Eidgenossenschaft
Confédération suisse
Confederazione Svizzera
Confederaziun svizra

Swiss Confederation

Federal Department of Economic Affairs, Education and Research EAER
State Secretariat for Education, Research and Innovation SERI

LEGAL NOTICE

DISCLAIMER

BAMBOO is funded by the European Union and the Swiss State Secretariat for Education, Research and Innovation (SERI). Views and opinions expressed are, however, those of the author(s) only and do not necessarily reflect those of the European Union, the European Research Executive Agency (REA), or SERI. Neither the European Union, SERI, nor the granting authority can be held responsible for them.

BAMBOO PARTNERS

NORGES TEKNISK-NATURVITENSKAPELIGE UNIVERSITET (NTNU)
Høgskoleringen 1, Trondheim 7491, Norway

UNIVERSITEIT LEIDEN (ULEI)
Rapenburg 70, 2311 EZ Leiden, Netherlands

WIRTSCHAFTSUNIVERSITÄT WIEN (WU)
Welthandelsplatz 1, 1020 Wien, Austria

EIDGENOESSISCHE TECHNISCHE HOCHSCHULE ZUERICH (ETH)
Raemistrasse 101, 8092 Zurich, Switzerland

MINISTERIE VAN INFRASTRUCTUUR EN WATERSTAAT (PBL)
Rijnstraat 8, 2500 EX Den Haag, Netherlands

AFRICA POLICY RESEARCH PRIVATE INSTITUTE GUG (APRI)
Brunnenstrasse 9, 10119 Berlin, Germany

PONTIFICIA UNIVERSIDAD CATÓLICA DEL PERU (PUCP)
Avenida Universitaria 1801 San Miguel, 15088 Lima, Peru

SOKOINE UNIVERSITY OF AGRICULTURE (SUA)
P.O. Box 3000, Chuo Kikuu, Morogoro, Tanzania

SGS PORTUGAL - SOCIEDADE GERAL DE SUPERINTENDÊNCIA S.A. (SGS)
Rua Cesina Adães Bermudes, Lote 11 nº1, Lisboa, Portugal

TABLE OF CONTENTS

BAMBOO PROJECT SUMMARY

Biodiversity and trade: mitigating the impacts of non-food biomass global supply chains

The **project's main goals** are to identify trade-offs between biodiversity impacts along global supply chains of non-food biomass and to determine leverage points for transformative change to halt and reverse biodiversity loss, both now and in the future. For this purpose, we develop new biodiversity impact assessment models, create a new, hybrid multiregional input-output (MRIO) model based on the well-known EXIOBASE and the biomass-specific FABIO models, and link the combined models to the integrated assessment model IMAGE for scenario generation. Apart from global assessments and recommendations, we showcase the applicability of our models in two local case studies of global relevance, fishmeal and fish oil production in Peru and cotton production in Tanzania, as well as two case studies with retailers.

Our project is **unique** in that we develop novel models to quantify biodiversity impacts using four indicators - species richness, mean species abundance, functional diversity, and ecosystem services - covering impacts across the terrestrial, freshwater, and marine realms. The hybrid MRIO model combines and extends existing physical and monetary MRIO models, allowing us to comprehensively track global flows of raw and processed non-food biomass in unprecedented detail. Using our system of coupled models, we assess the hotspots and leverage points of the non-food biomass economy and design future scenarios with mitigated impacts on ecosystems, identifying potential pathways for transformative change.

To facilitate transformative change towards protecting biodiversity, we develop an online tool that allows stakeholders to use all models easily. In general, our data will be freely available on Zenodo while safeguarding proprietary information from commercial partners. Overall, BAMBOO provides comprehensive and detailed knowledge of the effects of biomass trade from land and sea on biodiversity and ecosystem services and an improved way of identifying leverage points. This will ultimately contribute to better environmental decision-making by policymakers, retailers and other stakeholders, supporting the achievement of science-based targets and the SDGs.

EXECUTIVE SUMMARY

This report focuses on the development of a characterization factor model for ocean acidification within life cycle impact assessment (LCIA), as part of the broader BAMBOO project. Ocean acidification, accelerated by the absorption of greenhouse gasses, alters marine chemistry by reducing pH levels and diminishing carbonate availability, which is vital for marine ecosystems.

The study establishes a two-part model for endpoint characterization factors, the first part being a spatially explicit fate model that calculates midpoint characterization factors [pH·yr/kg_i] for 232 marine ecoregions and 18 FAO major fishing zones. This model quantifies how carbon dioxide (CO_2), carbon monoxide (CO), and methane (CH_4) emissions impact marine pH levels. The research expands on previous models by offering greater spatial detail, taking spatially heterogenous marine biogeochemical cycles into account and allowing for more precise calculations of the effect of emissions on the pH level of different ecosystems. The study also establishes a novel effect model with species sensitivity distributions that include a broader range of species than previous models. Combining the two, new endpoint characterization factors [PDF·yr/kg_i] are calculated that provide a more robust understanding of how emissions affect marine biodiversity through changes in ocean chemistry.

The results underscore the variability of ocean acidification effects across different ecosystems. For example, polar regions are more severely impacted due to their unique biogeochemical cycles, while equatorial regions experience less severe pH changes. The effect factors calculated in this report reflect these differences, highlighting the need for geographically specific mitigation strategies to protect vulnerable marine species and ecosystems.

The findings contribute to the broader goals of the BAMBOO project, which seeks to identify leverage points for reducing biodiversity loss in global biomass supply chains and provides a foundation for future research on mitigating ocean acidification and its impacts on marine life.

1 INTRODUCTION

The criticality of the ocean to life on earth as we know it is difficult to overstate. It provides a nearly endless myriad of services, from cultural to economic to biological. In recent decades there has been a push to realize the full potential of this "blue frontier", maximizing its economic output while preserving its ecological and cultural functions in line with the European Green Deal and the EU Blue Economy Policy, among other initiatives (Bennett et al., 2021; Ertör & Hadjimichael, 2020; Gamage, 2016). The ocean faces a similarly unsustainable level of anthropogenic pressures as the terrestrial realm, yet our knowledge of marine ecosystems and how human actions affect them is but a fraction of our understanding of the latter. This is reflected in life cycle impact assessment (LCIA), where marine impact models are significantly underrepresented compared to their terrestrial counterparts (Woods et al., 2016). The ability to quantify anthropogenic impacts on marine ecosystems is critical, especially as we continue to ramp up pressure on the oceans through the combination of marine economic exploitation and uncontrolled global warming.

One of the many critical services provided by the ocean is that of carbon sequestration. The ocean is the world's largest carbon sink, absorbing roughly 30% of anthropogenic greenhouse gas (GHG) emissions (Bach et al., 2016; Guinotte & Fabry, 2008). When greenhouse gases from the atmosphere meet the ocean surface, they react with water to produce carbonic acid, which then dissociates to form bicarbonate ions and protons (Feely et al., 2009). These subsequently react with carbonate ions to produce more bicarbonate ions (Feely et al., 2009). This process results in decreased pH and reduced availability of carbonate to biological systems.

Ocean acidification is becoming an increasingly urgent issue to address, as the current rate of acidification is unlike anything seen in at least 55 million years (potentially up to 300 million years) and only continues to accelerate (Findlay & Turley, 2021). Since pre-industrial measurements, marine pH has fallen by roughly 0.11 units (Doney et al., 2009; Guinotte & Fabry, 2008), and is predicted to decrease by another 0.3-0.4 units by the end of the century (Doney et al., 2009; Guinotte & Fabry, 2008) – a nearly 150% increase in acidification and the most rapid and severe

change marine ecosystems will have experienced in tens of millions of years (Feely et al., 2009; Findlay & Turley, 2021).

Marine organisms react in varied ways to ocean acidification and decreased carbonate availability. When it comes to biodiversity impacts, the largest body of research exists for calcifying species like corals, echinoderms, or bivalves. Calcifying species use carbonate to build their exoskeletons, and decreased availability of carbonate can lead to impacts including weaker shells/exoskeletons, reef collapse, and decreased hatch rates and larval survival (Doney et al., 2020; Findlay & Turley, 2021). Food web instability is also caused when calcifying keystone species, such as coccolithophores, are affected by decreased availability of carbonate (Doney et al., 2020). A growing body of research is also beginning to show that non-calcifying species, such as fish, are affected by ocean acidification through impacts including tissue acidosis, behavioral change, and reduced larval survival, among others (Doney et al., 2020; Radford et al., 2021).

Today, a spatially generic fate model exists for ocean acidification impacts from CO, CO_2, and CH_4 (Bach et al., 2016). In addition, spatially generic species sensitivity distributions (SSDs) for calcifying species exist (Azevedo et al., 2015), as well as an effect model that is spatially delineated for three regions and has separate effect factors for slightly and strongly calcifying species (Scherer et al., 2022). However, increased absorption of GHGs affects marine ecosystems differently across the globe. Complex biogeochemical cycles include factors such as carbonate chemistry variability, biological activity (photosynthesis and respiration), temperature and salinity, nutrient availability, geographic and seasonal variations, as well as human impacts and ecosystem disruption (Findlay & Turley, 2021, p. 13). Due to these factors, greenhouse gasses absorbed by the ocean will result in different changes in pH and carbonate availability in different geographical locations (Fabry et al., 2009; Ishii et al., 2020). Additionally, marine organisms react differently to changes in acidification. Organisms adapted to living in a high-variability or high-acidity environment may react less severely to increased acidification than those living in more stable or low-acidity conditions (Figuerola et al., 2021). For these reasons, spatially delineated characterization factors are critical for accurately quantifying marine impacts from ocean acidification. Additionally, an expanded representation of non- and slightly-calcifying species in effect models is required as a growing body

of research supports their inclusion in the damage caused by acidification.

The research conducted in this study aims to build upon the existing models by improving their coverage and accuracy through spatial delineation of the fate model and expansion of the effect model to more robustly cover slightly- and non-calcifying species and include greater spatial detail.

This study has also been accepted as a scientific article to Environmental Science and Technology as of October 7th, 2025 and should be published shortly.

2 METHODOLOGY

The life cycle impact assessment (LCIA) stage of LCA quantifies and interprets the environmental effects associated with a product or service over its lifetime (Joint Research Centre: Institute for Environment and Sustainability, 2011). This involves applying characterization factors (CFs) from impact models to translate emissions into impact category indicators. LCIA models can operate at the midpoint or endpoint level, where endpoints represent Areas of Protection such as ecosystem health (Joint Research Centre: Institute for Environment and Sustainability, 2011). Our ocean acidification model includes both levels and follows three main steps from emission to ecological impact (Figure 1):

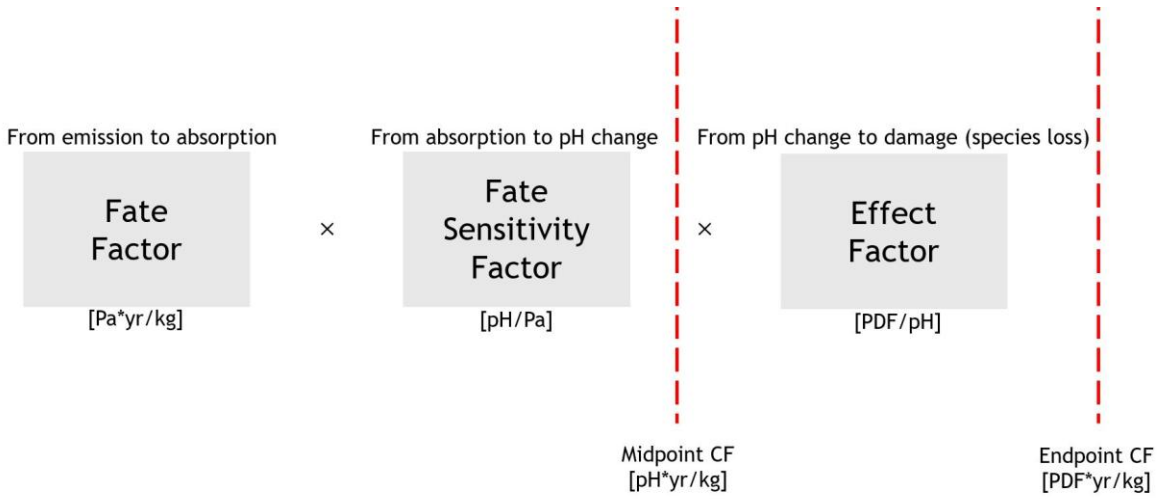

Figure 1. Model framework for mid- and endpoint characterization factors (CFs). Below each modeling step, the unit of the resulting factor is indicated in square brackets. PDF indicates the "potentially disappeared fraction of species" commonly used in LCIA models.

The fate factor links greenhouse gas emissions to changes in marine $spCO_2$; the

fate sensitivity factor describes how $spCO_2$ shifts affect pH; and the effect factor connects pH change to species-level impacts. The midpoint CF reflects marine pH change per kilogram emission, while the endpoint CF expresses ecosystem damage as the potentially disappeared fraction of species (PDF).

Data processing was performed in Python 3.13.0, ArcGIS Pro 3.3.0 (ESRI Inc., 2024), and R 4.4.1 (R Core Team, 2024). Details on the software packages used are provided in the Appendix (Section 1, Table S1).

2.1 Midpoint characterization factor model

The model for midpoint characterization factors (CFs) [pH·yr/kg_i] is made up of two components, the fate factor and the fate sensitivity factor:

$$CF_{midpoint,j,i} = FF_{j,i} \times (-FSF_j) \quad (1)$$

where the midpoint characterization factor [pH·yr/kg_i] for area *j* and substance *i* is the product of the fate factor (FF) [pH·yr/kg_i] for area *j* and substance *i* and the fate sensitivity factor (FSF) [pH/Pa] for area *j*. As the fate sensitivity factors are negative (reflecting the decline in pH), a negative sign is applied in the midpoint equation to ensure that the resulting characterization factors remain positive to indicate a net impact. Midpoint CFs have been calculated for the substances carbon dioxide (CO_2), carbon monoxide (CO), and methane (CH_4). They were spatially delineated for 232 marine ecoregions (Spalding et al., 2007) for coastal waters and 18 FAO major fishing areas (FAO, n.d.-a) for open ocean.

Marine ecoregions are biogeographic units of cohesive species composition, shaped predominantly by the same forcing agents included in marine biogeochemical cycles (i.e., upwelling, temperature, nutrient cycles, currents, etc.) (Spalding et al., 2007), and thus make a logical spatial unit for delineation. Lacking a similarly comprehensive biogeographic unit for open ocean, FAO major fishing areas were chosen. FAO major fishing areas are defined using inputs from international fisheries on both geopolitical and ecological boundaries (FAO, n.d.-b). For the FAO major fishing areas, the overlapping area with marine ecoregions was removed using ArcGIS to avoid double-counting.

2.1.1 Fate Factor

The fate factor quantifies the pathway from emission of GHGs to absorption by the environmental compartment (in this case, marine waters). By manipulating the Revelle Factor equation (a chemistry equation quantifying the buffer capacity of the marine carbonate system (Jiang et al., 2019)), it is possible to solve for the change in surface partial pressure CO_2 ($\Delta spCO2$) given a certain emission (Eq 2).

$$\Delta spCO2 = spCO2_{orig} * RF * (\frac{\Delta DIC}{DIC_{orig}}) \quad (2)$$

The variables DIC_{orig} (dissolved inorganic carbon) [mol/m^3] and $spCO2_{orig}$ (surface partial pressure CO_2) [Pa] are sourced from the Global Ocean Biogeochemistry Analysis and Forecast hosted on Copernicus, which is powered by the complex biogeochemical model NEMO v3.6 (*Global Ocean Biogeochemistry Analysis and Forecast*, n.d.). Monthly global values from November 2021 to December 2022 were downloaded with a resolution of 0.25 arc degrees. This date range was chosen to match Revelle Factor values as closely as possible. Values were then arithmetically averaged per marine ecoregion or FAO fishing zone.

Global surface ocean Revelle Factor (RF) values were sourced from National Oceanic and Atmospheric Administration (NOAA) Ocean Carbon and Acidification Data System (Jiang et al., 2019). The values are monthly, spanning the entirety of 2020, at a 1 arc degree resolution. The RF dataset was produced by combining present-day in situ measurements with an Earth system model and includes simulated values for Representative Concentration Pathways (RCPs) 2.6, 4.5, 6.0, and 8.5 (Jiang et al., 2019). For this study, RCP 4.5 was selected as it represents a stabilization pathway consistent with current emission trajectories under moderate mitigation (Jiang et al., 2019; van Vuuren et al., 2011). Revelle factor values were averaged across each spatial unit.

To assess the effect of this scenario choice, Revelle factors and midpoint characterization factors (CFs) under RCP 4.5 and RCP 6.0 were compared. The mean difference in Revelle factor between RCP 6.0 and 4.5 was −0.0027, corresponding to an average CF change of -2.49×10^{-17}. This equates to a sensitivity of 2.92×10^{-15} impact units per unit change in Revelle factor. In practical terms, even a full unit shift in the Revelle factor would cause a negligible difference in midpoint CFs, confirming that these factors are largely insensitive to small variations across mid-range RCP scenarios.

ΔDIC in equation 2 can be represented with equation 3, given an emission of substance *i* (Eq 3):

$$\Delta DIC = \frac{(\frac{\Delta E_i * DF_i}{M_{CO2}})}{a} \quad (3)$$

The dissolution factor (DF_i) [-] in equation 3 quantifies how much of the emission of substance *i* (ΔE_i) [kg_i/yr] will eventually dissolve in the ocean as CO_2. These values are calculated from the spatially generic fate model pathway by Bach et al. (2016) (Table 1, Fig 1).

Table 1. Dissolution factors [-] for CO_2, CO, and CH_4.

Substance	Dissolution factor
Carbon dioxide (CO_2)	0.27225
Carbon monoxide (CO)	0.23713
Methane (CH_4)	0.22708

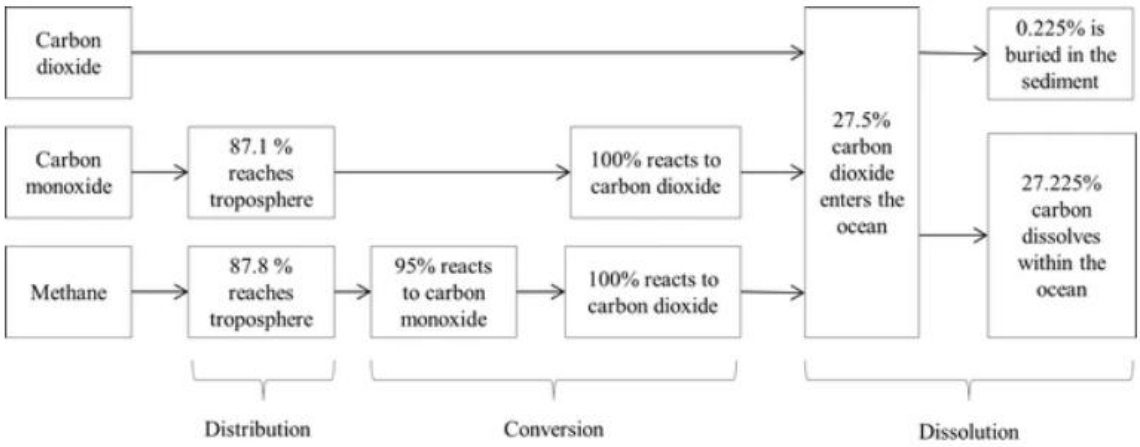

Figure 2. Ocean acidification fate pathway for CO2, CO, and CH4 (Bach et al., 2016).

CO and CH_4 both convert to carbon dioxide in the troposphere before contributing to ocean acidification as CO_2 dissolving with seawater (Bach et al., 2016). Therefore only one molar mass constant (M_{CO2}) [kg/mol] is used, that of CO_2, given as 4.4E-02 kg/mol (PubChem, n.d.). The dissolution factors account for the conversion of CO and CH_4 to CO_2. It is assumed that an emission will be well-mixed and may be absorbed by the ocean at any location, thus *a* represents the surface volume of the open ocean free of ice shelves, equaling 361 × 10^6 m^3 (Cogley, 2012).

2.1.2 Fate Sensitivity Factor

The fate sensitivity factor reflects the change in a considered environmental compartment when an emitted substance enters it. This was calculated using linear regression modeling of the relationship of pH with respect to $spCO_2$. This was done for each marine ecoregion and each FAO fishing zone individually. pH values were also sourced from the Global Ocean Biogeochemistry Analysis and Forecast hosted on Copernicus, powered by NEMO v3.6 (*Global Ocean Biogeochemistry Analysis and Forecast*, n.d.). Monthly global values from November 2021 to December 2022 were downloaded with a resolution of 0.25 degrees. The same $spCO_2$ dataset used in the fate factor calculations was also used for calculating the fate sensitivity factor.

2.1.3 Midpoint Characterization Factors

Lastly, midpoint characterization factors [pH·yr/kg_i] were calculated by multiplying the fate [Pa·yr/kg_i] and fate sensitivity factors [pH/Pa] for each emission substance (Eq 1). In total, 750 CFs were produced, representing 232 marine ecoregions and 18 FAO fishing areas for each of the three analyzed GHGs.

The area of each spatial unit was calculated in km^2 using geodesic measurements on the ellipsoid in EPSG:4326 and applied as weights to derive globalized midpoint CFs. The aggregated CFs ($CF_{agg,i}$) were subsequently normalized to the reference gas, CO_2, to express final global CFs in CO_2-equivalents ($CF_{norm,i}$):

$$CF_{norm,i} = \frac{CF_{agg,i}}{CF_{agg,CO2}} \quad (4)$$

2.2 Effect Factor Model

Endpoint characterization factors (CFs) were obtained by combining the spatially explicit midpoint CFs with spatialized effect factors at the level of FAO regions or marine ecoregions. Effect factors translate midpoint impacts into endpoint damages, expressed here as the potentially disappeared fraction of species (PDF).

To estimate species sensitivity to pH changes, the species sensitivity distribution (SSD) method was applied. SSDs determine the pH level that is hazardous to x% of species (HC_x). Experimental data describing species' responses to acidification were used to construct the SSD curves. Following the approach of Azevedo et al. (2014),

we derived the pH at which 50% (pH_{50}) and 10% (pH_{10}) reductions in key biological traits (e.g., growth or reproduction) occur for each dataset. Logistic regression was employed to fit response curves and estimate these values.

The resulting HC_x values derived from the SSDs were then used to calculate the corresponding effect factors (Eqs. 8 and 9).

2.2.1 Data Collection

To capture species responses to varying levels of ocean acidification across diverse regions and calcification types, we used a dataset compiled by the Ocean Acidification International Coordination Centre (OA-ICC) and hosted on PANGAEA (Felden et al., 2023). The compilation contains over 1,500 experiments published between 2008 and 2023 examining the effects of ocean acidification on marine organisms. Experiments involving kingdoms other than animalia and/or testing multiple stressors (e.g., combining acidification with elevated temperatures or increased metal toxicities) were excluded. To apply the logistic regression approach for deriving pH_{50} and pH_{10} values (the pH levels at which 50% and 10% of individuals experience a reduction in key traits such as growth or reproduction), each experiment was required to include at least three distinct pH test conditions, as the model involves two parameters and one degree of freedom. After filtering, this search yielded a subset of 24 usable studies with response data for 32 species in total (see Appendix, Section 2).

To ensure representation of a variety of species, studies were classified by calcification level, region, and trophic level (Tables 2-3). For calcification level, we have defined strongly calcifying species as species that have major external calcifying elements (i.e. carbonate exoskeleton or shell), slightly calcifying species as having major internal calcifying elements (i.e. carbonate cuttlebone or endoskeleton), and non-calcifying species as having minor internal calcifying elements (i.e. otoliths or calcareous spicules). Although nearly every species has some kind of calcifying biological function, we have decided to call the lowest calcification category “non-calcifying” in line with existing literature (Kroeker et al., 2010). For the effect factor calculation we delineated 4 climate zones: polar, temperate, sub-tropical, and tropical (Rohli et al., 2015). Three trophic levels were

considered: primary consumers (level 2), secondary consumers (level 3), and tertiary consumers (level 4). Trophic level 1 (primary producers, mainly plankton and algae) and level 5 (apex predators such as sharks and whales) were excluded due to a lack of suitable single-stressor experimental data. The absence of these groups represents a limitation and should be considered when comparing endpoint results across species sets.

Table 2. Total species representation in each calcification and region category.

	Calcification			**Region**			
	Non	Slightly	Strongly	Polar	Temperate	Sub-Tropical	Tropical
Total	10	6	16	7	19	15	13

Table 3. Total species representation in each trophic level.

	Trophic Level		
	Primary Consumer	Secondary Consumer	Tertiary Consumer
Total	20	7	5

2.2.2 Derivation of pH_{50} and pH_{10} Values

Within this study, the methodology presented by Azevedo et al. (2014) was used to derive the pH at which a 50%-reduction of a vital trait (such as growth or reproduction) occurs (pH_{50}), as well as the pH at which a 10%-reduction of a vital trait occurs (pH_{10}) for each experiment. This was done by first calculating the empirical relative response (eRR), a normalized response rate:

$$eRR_t = 1 - \frac{R_c}{R_t} \quad (5a)$$

where R_c is the reference response at pH *c* (the control condition) and R_t is the relative response at pH *t* (the test condition). Eq 5a represents a scenario where reduction of a vital trait is represented by an increasing response, for example bioerosion rate. If the experiment reported reduced function (e.g., reduced calcification, fertilization rate, degustation rate) rather than increased function, the equation was modified:

$$eRR_t = 1 - \frac{R_t}{R_c} \quad (5b)$$

where the relative response at pH t (R_t) is now the numerator and the reference response at pH c (R_c) is now the denominator.

Next, eRR_t and corresponding pH_t values were used to fit a logistic regression with the output variables pH_{50} and ß:

$$cRR_t = \frac{1}{1+10^{(pH_{50}-pH_t/\beta)}} \quad (6)$$

where cRR_t is the calculated relative response for pH t, pH_{50} is the pH at which a 50%-reduction occurs in a vital function of the studied species, and ß is the slope of the logistic regression. In line with precautionary principle, it is now recommended to use the effect concentration where a 10%-reduction occurs in a vital function (Owsianiak et al., 2023), thus the pH_{10} value was also calculated using the previously derived pH_{50} and ß values:

$$pH_{10} = \beta \times \log_{10} 9 + pH_{50} \quad (7)$$

2.2.3 Species Sensitivity Distributions

SSD (Species Sensitivity Distribution) curves are commonly used to estimate the sensitivity of various species to an environmental stressor, such as ocean acidification, by representing the cumulative proportion of species affected at different concentrations. The SSD curve is then used to determine the hazardous concentration (HC), such as HC20 or HC50, which indicate the pH levels at which 20% or 50% of species are affected, respectively. These HC values can then be used to calculate effect factors. In life cycle impact assessment, it is common to use HC50 values when creating effect factors (Owsianiak et al., 2023). However, there is growing support for using a lower threshold such as HC20, as HC50 levels are often well beyond environmentally relevant concentrations (Owsianiak et al., 2023). In this study, we have created SSD curves following the historical precedent of using HC50 values, and we have also included an approach recommended by Owsianiak et al. (2023) using the value at $HC20_{EC10}$. This approach uses EC10 values (what we call pH_{10} in this study; the pH at which there is a 10%-reduction in the studied vital function of a species) to build the SSD curve and takes the HC20 value, at which 20% of species are affected at their EC10 (in our case pH_{10}) level.

The SSD curves were constructed in R version 4.4.1 (R Core Team, 2024). pH_{50} or pH_{10} values were used to calculate cumulative proportions, and a logistic regression model with a quasibinomial logit link was used to fit the SSD curve to the pH concentration data. The SSD curves contain data points for 32 different species, encompassing 3 different trophic levels. Two global SSD curves have been constructed, one for $HC50_{pH50}$ and one for $HC20_{pH10}$, as well as three SSD curves for strongly, slightly, and non-calcifying organisms, and four SSD curves for tropical, subtropical, temperate, and polar regions.

2.2.4 Effect Factor

Our approach differs from standard ecotoxicological methods for calculating effect factors in two key ways. First, typical ecotoxicology studies define a clear baseline or "zero exposure" condition, which is often assumed to be the absence of a contaminant. However, for ocean acidification it is not meaningful to define a zero-exposure state, as pH is an inherent property of the marine system. Instead, we adopt a reference state representing pre-industrial ocean conditions, consistent with approaches used in other impact categories such as land use. Historical ocean pH values from Jiang et al. (2019) were used for this purpose; their dataset provides monthly global pH estimates for the year 1770 at a 1° spatial resolution. The global arithmetic mean pH was calculated to be 8.19 and used as the reference condition.

Second, in conventional ecotoxicology, higher tolerated exposure levels indicate lower species sensitivity. For ocean acidification, the relationship is reversed: species that tolerate lower pH (i.e., more acidic conditions) are considered less sensitive. To address this, we follow the precedent of eutrophication models dealing with dissolved oxygen (DO), which encounter a similar inverse relationship (Cosme et al., 2020). Sensitivity is based on the difference (ΔpH) between the reference state and the hazardous concentration (HC) value. The effect factor [PAF/pH] was then calculated using the $HC20_{pH10}$ value according to Equation 8:

$$EF_{20} = \frac{0.20}{pH_{orig} - HC20_{pH10}} \quad (8)$$

Following historical precedent, the effect factor was also calculated using the $HC50_{pH50}$ value, using equation 8:

$$EF_{50} = \frac{0.50}{pH_{orig} - HC50_{pH50}} \quad (9)$$

Effect factors were calculated using each of the SSD curves for calcification and region, resulting in 16 effect factors in total. The global effect factor from equation 8 (EF_{20}) was used to calculate endpoint characterization factors as it has the highest representation of species.

The Potentially affected fraction (PAF) is transformed to the generally used potentially disappeared fraction (PDF) with an assumption of 1:1 (i.e. species that are affected will also disappear). This is based on the recommendations of the life cycle initiative hosted by UN Environment, GLAM project. The recommendation for this 1:1 exchange is based on work from Oginah (2023).

2.3 Endpoint Characterization Factors

Endpoint characterization factors were calculated using equation 8:

$$CF_{endpoint,j,c,i} = FF_{j,i} \times (-FSF_j) \times EF_{j,c} \quad (10)$$

Where the endpoint characterization factor for area *j*, calcification level *c*, and substance *i* is equal to the fate factor for area *j* and substance *i* ($FF_{j,i}$) multiplied with fate sensitivity factor for area *j* (FSF_j) and the effect factor for area *j* and calcification level *c* ($EF_{j,c}$). The endpoint CF unit is potentially disappeared fraction of species per kilogram emission of substance *i* [PDF·yr/kg_i]. Calculations were completed in Excel and resulted in 750 endpoint characterization factors; 232 for marine ecoregions and 18 for FAO fishing areas, for each of the three GHGs. A globally aggregated endpoint CF was also calculated by taking the area of each spatial unit in km^2 in ArcGIS Pro and using it to weight the globalized endpoint CFs.

3 RESULTS

3.1 Midpoint Characterization Factor Model

3.1.1 Fate Factor

The fate factor quantifies the pathway from emission to absorption by the environmental compartment. There are three different sets of fate factors, one for each emission substance (CO_2, CO, and CH_4). Figure 3B shows the fate factor values

for CO_2, which range from 5.76E-12 Pa/kg (most severe) to 2.50E-12 Pa/kg (least severe). The values for CO range from 5.01E-12 Pa $spCO_2$/kg to 2.18E-12 Pa $spCO_2$/kg, and for CH_4 from 4.80E-12 Pa $spCO_2$/kg to 2.09E-12 Pa $spCO_2$/kg.

The value distribution shows more extreme reactions at polar latitudes and less severe reactions closer to the equator and follows the same pattern for each substance. All fate factor values can be found in Tables S2-3 in the appendix.

3.1.2 Fate Sensitivity Factors

The fate sensitivity factor reflects the change in a considered environmental compartment when an emitted substance enters it. There is only one set of fate sensitivity factors as all considered GHGs convert to CO_2 in the troposphere (Bach et al., 2016). The fate sensitivity factors range from 1.60E-02 pH/Pa $spCO_2$ (most severe) to 1.47E-04 pH/Pa $spCO_2$ (least severe). The fate sensitivity factors generally follow expected patterns, with outliers near the Antarctic and Greenland coasts. All fate sensitivity factor values are pictured in Figure 3C and can be found in Tables S4-5 in the appendix.

3.1.3 Midpoint Characterization Factors

The midpoint characterization factors for CO_2 are pictured in figure 3A and ranged from 9.16E-14 pH/kg (most severe) to 4.72E-16 pH/kg (least severe), for CO from 7.98E-14 pH/kg to 4.11E-16 pH/kg, and for CH_4 from 7.64E-14 pH/kg to 3.94E-16 pH/kg. As with the fate factor and fate sensitivity factor, they generally follow expected patterns of severity. All midpoint characterization factors can be found in Tables S6-7 in the Appendix. The global, normalized midpoint CFs, set in relation to the reference substance CO_2, are 1 kg CO_2 Eq/kgCO2, 0.87 kg CO_2 Eq/kg_{CO}, and 0.83 kg CO2 Eq/kg_{CH4}.

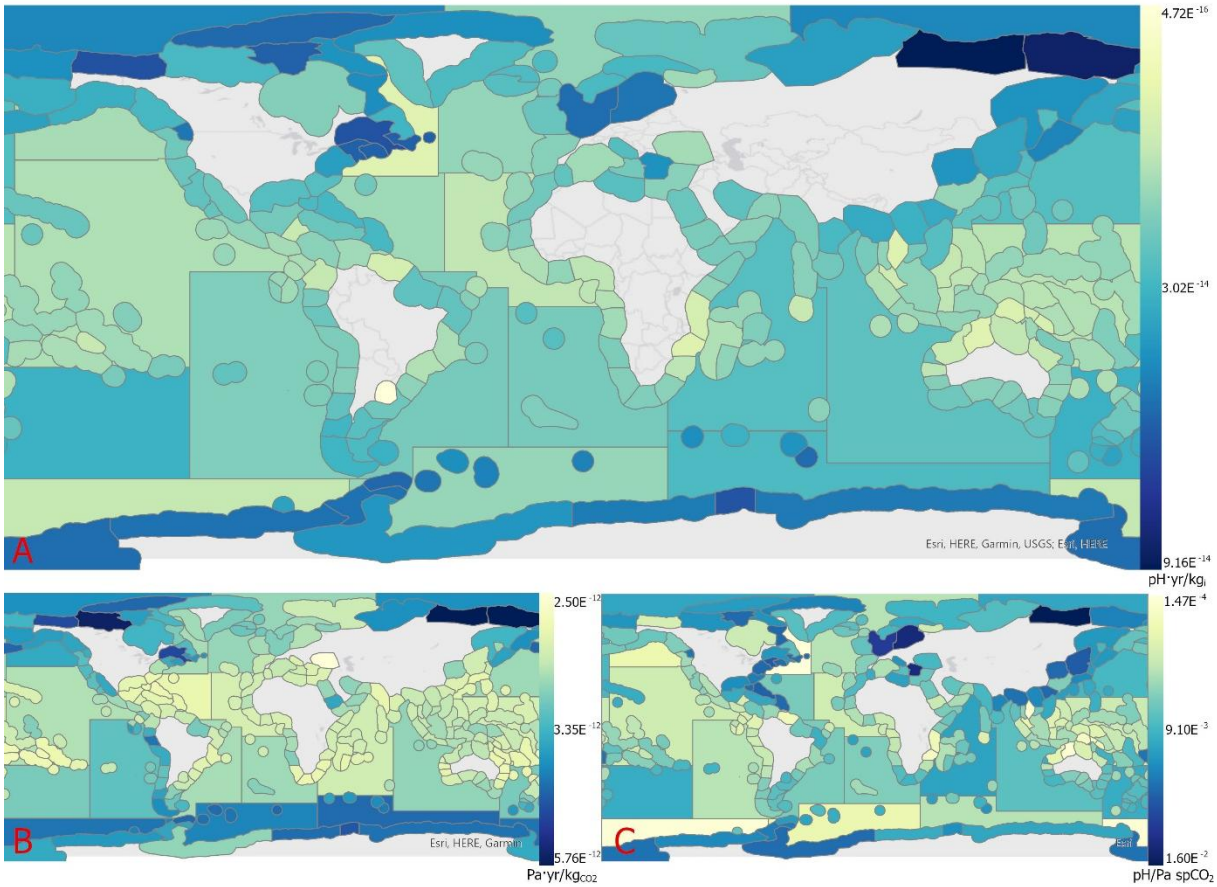

Figure 3A-C. Figure A is the change in pH per kilogram CO2 emitted [pH yr/kg] (midpoint CFco2) in FAO major fishing zones and marine ecoregions. Figure B is the average change in spCO2 [Pa/m3] per kg CO2 emitted (Fate Factor). Figure C is the average change in marine pH per unit increase of spCO2 [Pa/m3] (Fate Sensitivity Factor). Continent basemap from ESRI (2024).

3.2 Effect Factor Model

3.2.1 Species Sensitivity Distributions

SSD curves were fitted for two hazardous concentration levels: $HC50_{pH50}$ and $HC20_{pH10}$. Both curves have 32 data points representing 32 different species belonging to three different trophic levels and six phyla.

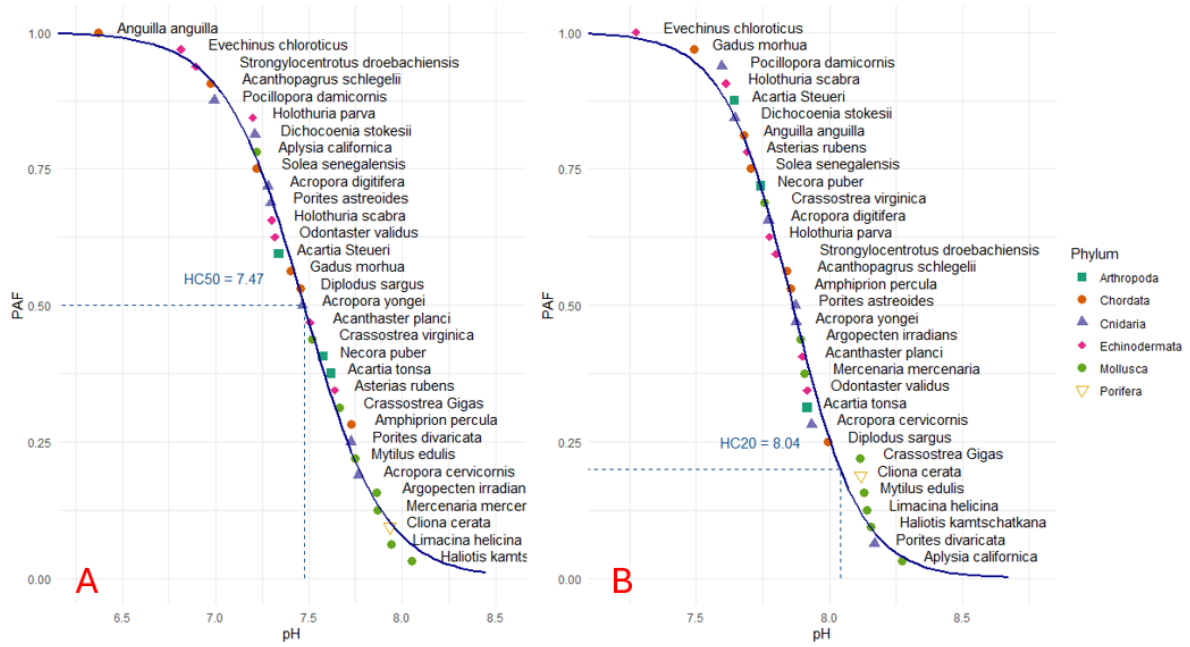

Figure 4A-B. Figure A pictures species sensitivity distribution of the pH50 values for 32 different marine species. Figure B pictures species sensitivity distribution of the pH10 values for 32 different marine species.

In figure 4A, pH_{50} values (the pH at which a 50%-reduction occurs in a vital function) are plotted and the HC50 is derived as 7.47. As a reminder, the HC50 represents the pH value at which 50% of species studied reach their pH_{50}.

In figure 4B, pH_{10} values (the pH at which a 10%-reduction occurs in a vital function) are plotted and the $HC20_{pH10}$ is derived as 8.04.

SSD curves were also fitted for 3 calcification levels: strongly calcifying, slightly calcifying, and non-calcifying. (Appendix, figures S2-4), and for 4 regional levels: tropical, subtropical, temperate, and polar (Appendix, figures S5-8)

3.2.2 Effect Factor

Sixteen effect factors have been calculated; two at the global level, six at the calcification level, and eight at the region level. The global EFs contain all 32 species. The global EF_{20} (1.35 PDF/pH) was used in the calculation of endpoint characterization factors.

		EF20 [PDF/pH]	EF50 [PDF/pH]
	Global	1.35E+00	7.00E-01
Calcification	**Strongly**	2.46E+00	8.70E-01

	Slightly	2.77E+00	6.18E-01
	Non	9.82E-01	6.63E-01
Region	**Tropical**	1.05E+00	6.72E-01
	Subtropical	1.48E+00	6.98E-01
	Temperate	1.84E+00	7.33E-01
	Polar	2.61E+00	7.37E-01

3.3 Endpoint Characterization Factor Model

The endpoint characterization factors for CO_2 ranged from 1.23E-13 PDF yr/kg (most severe) to 6.36E-16 PDF yr/kg (least severe), for CO from 1.07E-13 PDF yr/kg to 5.54E-16 PDF yr/kg, and for CH_4 from 1.03E-13 PDF yr/kg to 5.30E-16 PDF yr/kg. All endpoint characterization factors can be found in Tables S8-9 in the appendix.

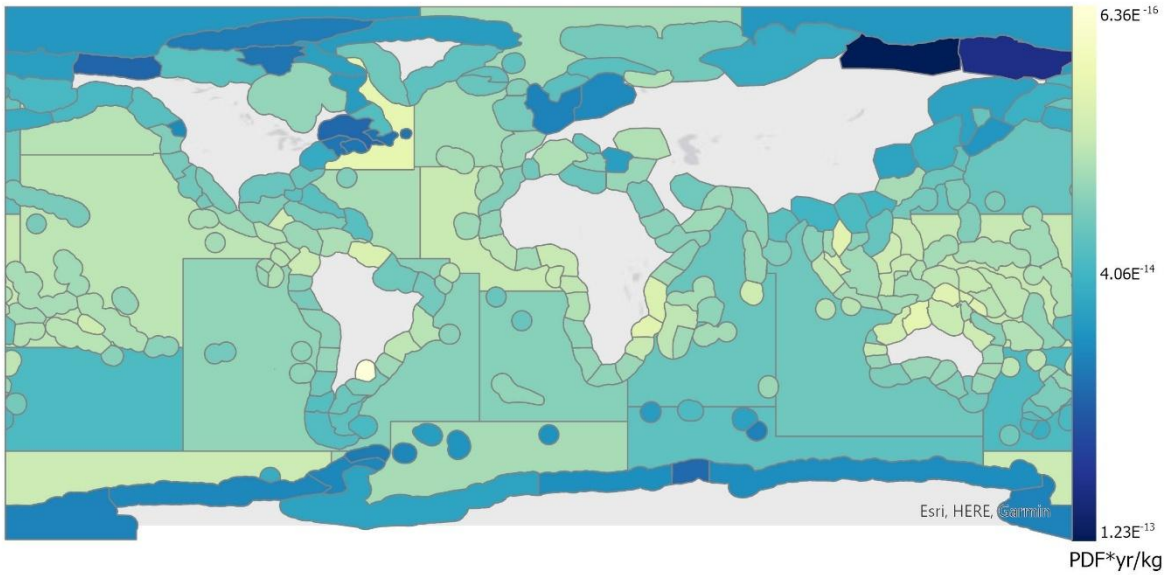

Figure S9: Visualization of endpoint characterization factors for CO_2. Change in PDF per kilogram CO2 emitted [PDF yr/kg] (endpoint CFco2) in FAO major fishing zones and marine ecoregions.

4 DISCUSSION

Biogeochemical cycles in the ocean are complex, with far-reaching effects and feedback mechanisms that are only partially understood. Variables such as

temperature, salinity, nutrient availability, and redox conditions all influence acidification dynamics (Findlay & Turley, 2021, p. 13). Ocean acidification is most drastic at polar latitudes, specifically northern latitudes (the arctic), due to the sensitivity of acid-base dissociation at cold temperatures and naturally low carbonate ion concentrations (Fabry et al., 2009). Equatorial regions exhibit greater buffering capacity against increased pCO_2 due to strong carbonate saturation, upwelling of lower-pCO_2 waters, and high biological uptake of dissolved inorganic carbon (DIC) (Ishii et al., 2020).

Our midpoint characterization factors (CFs) reflect these expected global patterns, with higher values near the poles and lower values around the equator (Figure 3A). Some notable regional outliers were also observed. Exceptionally severe fate sensitivity factors occurred along the North American east coast and in the Baltic Sea, corresponding with areas known for severe hypoxia and dead zones (Altieri & Gedan, 2015). The respiration of algal blooms and other organisms under hypoxic conditions generates additional CO_2, which locally decreases pH—an effect captured by the datasets used to derive the fate sensitivity factors. Outliers with lower than expected FSFs were also identified in the Labrador Sea and Southern Ocean, where regional anomalies such as low salinity, oxygen disequilibria, and complex circulation patterns likely influence pH response (Fox et al., 2022; Gille et al., 2022; Silva et al., 2024).

Within the midpoint CF model, several data limitations affect accuracy and coverage. The fate model relies on surface-level pCO_2 data (to depths of ~50 m), which constrains representation of subsurface conditions. pH typically declines with depth due to CO_2 released by biological respiration and vertical mixing (Findlay & Turley, 2021). Of the species included in the effect model, four inhabit non-coastal benthic environments (three Echinodermata and one Porifera), meaning their modeled impacts may be more uncertain. Incorporating depth-resolved pCO_2 data in future work—potentially through bathymetric averaging or depth-stratified CFs (e.g., coastal, pelagic, benthic)—could improve model fidelity.

Including depth could also refine the spatial delineation used. Variability analysis indicated that FAO fishing areas, although larger than marine ecoregions (MERs), were more homogeneous (Appendix Figure S1). If vertical variation were introduced,

a finer regional resolution might be more appropriate for open-ocean regions, where benthic conditions are likely more heterogeneous.

Furthermore, while atmospheric impact models typically assume that greenhouse gases (GHGs) are evenly distributed ("well-mixed"), marine interactions with atmospheric CO_2 are influenced by both spatial and temporal factors. Introducing an atmospheric distribution component into the fate factor could improve accuracy by accounting for regional variations in ocean-atmosphere contact zones.

It is important to note that the midpoint CFs in this study quantify the expected pH change per kilogram of CO_2 emitted, based on specific regional and temporal conditions. Practitioners can update these factors by recalculating Equations (2) and (3) with contemporary $spCO_2$, pH, Revelle Factor, and DIC data. While annual variation is likely small, long-term shifts could be substantial. The CFs thus represent localized, short- to medium-term effects and do not fully capture the broader carbonate buffering capacity or long-term feedback mechanisms of the ocean system. Acid-base reactions forming DIC occur on timescales of seconds (Feely et al., 2009), atmosphere–ocean equilibration over months (Feely et al., 2009), and biological carbon cycling over seasons or years (Mostofa et al., 2016). Consequently, the model represents immediate and intermediate dynamics rather than long-term feedbacks that may alter ocean CO_2 uptake capacity.

The species sensitivity distributions (SSDs) follow expected patterns, with strongly calcifying species being most vulnerable to acidification and non-calcifying species being least affected. Regional SSDs would benefit from expanded polar data to strengthen geographic comparisons. Among the calcification categories, the "slightly calcifying" group exhibits the highest uncertainty due to limited data. Nevertheless, this intermediate category enhances ecological realism beyond a simple "calcifying/non-calcifying" dichotomy and provides a useful foundation for future refinements.

Developing SSDs that compare regions with high natural pH variability (e.g., intertidal zones) to those with more stable pH conditions could yield further insights. Species from fluctuating environments may exhibit greater tolerance to acidification than those from more stable settings (Duarte et al., 2013; Edworthy et al., 2024; Pansch et al., 2014; Vargas et al., 2017). It is also important to acknowledge that

roughly 12% of reviewed studies found neutral or even positive short-term responses to lower pH, possibly due to temporary metabolic overcompensation (e.g., increased feeding or growth) that may not be sustainable over multiple generations (Edworthy et al., 2024; Pansch et al., 2014). This demonstrates that while ocean acidification's negative effects on strongly calcifying species are well established, the responses of slightly and non-calcifying taxa are still being understood.

The range of endpoint CFs produced in this study highlights the spatial variability of marine ecosystem sensitivity to acidification—reflecting regional ocean chemistry, ecological composition, and species-specific responses. Including diverse taxa ensures that both direct and indirect biological sensitivities are represented, improving ecological relevance. These CFs can be applied to any life cycle inventory containing CO_2, CO, or CH_4 emissions to air.

Such spatially explicit models are critical for developing targeted mitigation strategies and enhancing marine representation in life cycle impact assessment (LCIA) frameworks, which currently underrepresent marine categories (e.g., GLAM and LC-IMPACT include only one or two). Using our CFs, a practical example can be drawn from the maritime shipping sector, which emitted approximately 820 million tonnes of CO_2 in 2023. Applying our ocean acidification endpoint CF alongside LC-IMPACT's climate change CF yields 3.48×10^{-3} PDF·yr from acidification and 1.44×10^{-3} PDF·yr from climate change. The PDF·yr metric represents the proportion of species under threat over time; in this case, roughly 0.35% of species would face pressure equivalent to one year of disappearance risk. These results suggest that ocean acidification poses approximately 2.5 times greater biodiversity risk than climate change for equivalent CO_2 emissions.

Carbon dioxide is the main source of ocean acidification (and therefore also greenhouse gasses that devolve into carbon dioxide, such as carbon monoxide and methane). However, there are a number of terrestrial substances that also contribute to coastal marine acidification through leaching, including nitrogen oxides (NOx) and sulfur dioxides (SO_2) (Bach et al., 2016; Scherer et al., 2022). There have been suggestions for how to include these substances in an ocean acidification impact model (Bach et al., 2016); however, due to the small contribution relative to GHGs, it was decided to continue only with the specified atmospheric emissions.

The results of this study will be used in the update of LC-IMPACT that comprises task 1.5 in work package 1 of BAMBOO. The characterization factors developed here will also be used in work packages 3 and 4 in the assessment of leverage points for biodiversity conservation. The results have been developed in collaboration with partners from the appropriate work packages to ensure downstream compatibility.

5 CONCLUSION

The oceans, and all the services they provide for us, are under growing pressure. As greenhouse gas emissions rise, ocean acidification becomes an increasingly pressing threat to marine ecosystem function. The chemical mechanisms driving ocean acidification have been well understood for decades, but research on how it affects marine biology and ecosystems has expanded rapidly in recent years and continues to evolve. Some generalizations are established—such as strongly calcifying species being more sensitive to ocean acidification—but overall generalizations are difficult to apply. Complex mechanisms including natural pH fluctuations, life stage, and co-stressors influence species sensitivity in ways that are not yet fully understood.

This makes it particularly important to control for the elements that are better characterized, such as the spatial dynamics of ocean acidification. Our study addresses this research gap through the development of spatially explicit midpoint and endpoint models that account for spatial variability across 232 coastal marine ecoregions and 18 FAO major fishing zones, alongside an effect model representing species from a range of regions and calcification levels. Results follow the pattern predicted by literature, with more severe acidification at polar latitudes and milder impacts near equatorial regions, further supporting the need for the spatial differentiation provided here.

Anthropogenic pressures on the ocean are growing rapidly, even as policies such as the EU's Blue Economy emphasize the need to preserve marine environments. These dual realities underscore the importance of integrating marine models into life cycle impact assessment (LCIA). Our model can be incorporated into commonly used LCIA frameworks to help address the underrepresentation of marine impacts

and to provide a more robust, spatially defined understanding of how best to mitigate the marine consequences of greenhouse gas emissions.

6 REFERENCES

Altieri, A. H., & Gedan, K. B. (2015). Climate change and dead zones. *Global Change Biology*, *21*(4), 1395–1406. https://doi.org/10.1111/gcb.12754

Azevedo, L. B., De Schryver, A. M., Hendriks, A. J., & Huijbregts, M. A. J. (2015). Calcifying Species Sensitivity Distributions for Ocean Acidification. *Environmental Science & Technology*, *49*(3), 1495–1500. https://doi.org/10.1021/es505485m

Bach, V., Möller, F., Finogenova, N., Emara, Y., & Finkbeiner, M. (2016). Characterization model to assess ocean acidification within life cycle assessment. *The International Journal of Life Cycle Assessment*, *21*(10), 1463–1472. https://doi.org/10.1007/s11367-016-1121-x

Bennett, N. J., Blythe, J., White, C. S., & Campero, C. (2021). Blue growth and blue justice: Ten risks and solutions for the ocean economy. *Marine Policy*, *125*, 104387. https://doi.org/10.1016/j.marpol.2020.104387

Cogley, J. G. (2012). Area of the Ocean. *Marine Geodesy*, *35*(4), 379–388. https://doi.org/10.1080/01490419.2012.709476

Cosme, N., Verones, F., & Hauschild, M. Z. (2020). Marine Eutrophication. *LC-Impact Version 0.1*, *1*.

Doney, S. C., Busch, D. S., Cooley, S. R., & Kroeker, K. J. (2020). The Impacts of Ocean Acidification on Marine Ecosystems and Reliant Human Communities. *Annual Review of Environment and Resources*, *45*(Volume 45, 2020), 83–112. https://doi.org/10.1146/annurev-environ-012320-083019

Doney, S. C., Fabry, V. J., Feely, R. A., & Kleypas, J. A. (2009). Ocean Acidification: The Other CO_2Problem. *Annual Review of Marine Science*, *1*(1), 169–192. https://doi.org/10.1146/annurev.marine.010908.163834

Duarte, C. M., Hendriks, I. E., Moore, T. S., Olsen, Y. S., Steckbauer, A., Ramajo, L., Carstensen, J., Trotter, J. A., & McCulloch, M. (2013). Is Ocean Acidification an Open-Ocean Syndrome? Understanding Anthropogenic Impacts on Seawater pH. *Estuaries and Coasts*, *36*(2), 221–236. https://doi.org/10.1007/s12237-013-9594-3

Edworthy, C., James, N. C., Potts, W. M., Duncan, M. I., & Dupont, S. (2024). Temperate coastal fish shows resilience to extreme low pH in early larval stages. *Journal of Experimental*

Marine Biology and Ecology, *578*, 152037. https://doi.org/10.1016/j.jembe.2024.152037

Ertör, I., & Hadjimichael, M. (2020). Editorial: Blue degrowth and the politics of the sea: rethinking the blue economy. *Sustainability Science*, *15*(1), 1–10. https://doi.org/10.1007/s11625-019-00772-y

ESRI Inc. (2024). *ArcGIS Pro* (Version 3.3.0) [Computer software].

Fabry, V. J., Mcclintock, J. B., Mathis, J. T., & Grebmeier, J. M. (2009). Ocean Acidification at High Latitudes: The Bellwether. *Oceanography*, *22*(4), 160–171.

FAO. (n.d.-a). *FAO Fisheries and Aquaculture Catalogue—FAO - Fisheries and Aquaculture Division, n.d.* Retrieved September 25, 2024, from https://www.fao.org/fishery/geonetwork/srv/eng/catalog.search#/metadata/ac02a460-da52-11dc-9d70-0017f293bd28

FAO. (n.d.-b). *Main water areas | Coordinating Working Party on Fishery Statistics (CWP) | Food and Agriculture Organization of the United Nations*. Retrieved September 25, 2024, from https://www.fao.org/cwp-on-fishery-statistics/handbook/general-concepts/main-water-areas/en/

Feely, R. A., Doney, S. C., & Cooley, S. R. (2009). Ocean Acidification: Present Conditions and Future Changes in a High-CO_2 World. *Oceanography*, *22*(4), 36–47.

Felden, J., Möller, L., Schindler, U., Huber, R., Schumacher, S., Koppe, R., Diepenbroek, M., & Glöckner, F. O. (2023). PANGAEA - Data Publisher for Earth & Environmental Science. *Scientific Data*, *10*(1), 347. https://doi.org/10.1038/s41597-023-02269-x

Figuerola, B., Hancock, A. M., Bax, N., Cummings, V. J., Downey, R., Griffiths, H. J., Smith, J., & Stark, J. S. (2021). A Review and Meta-Analysis of Potential Impacts of Ocean Acidification on Marine Calcifiers From the Southern Ocean. *Frontiers in Marine Science*, *8*. https://doi.org/10.3389/fmars.2021.584445

Findlay, H. S., & Turley, C. (2021). Ocean acidification and climate change. In T. M. Letcher (Ed.), *Climate Change (Third Edition)* (pp. 251–279). Elsevier. https://doi.org/10.1016/B978-0-12-821575-3.00013-X

Fox, A. D., Handmann, P., Schmidt, C., Fraser, N., Rühs, S., Sanchez-Franks, A., Martin, T., Oltmanns, M., Johnson, C., Rath, W., Holliday, N. P., Biastoch, A., Cunningham, S. A., & Yashayaev, I. (2022). Exceptional freshening and cooling in the eastern subpolar North

Atlantic caused by reduced Labrador Sea surface heat loss. *Ocean Science*, *18*(5), 1507–1533. https://doi.org/10.5194/os-18-1507-2022

Gamage, R. N. (2016). Blue economy in Southeast Asia: Oceans as the new frontier of economic development. *Maritime Affairs: Journal of the National Maritime Foundation of India*, *12*(2), 1–15. https://doi.org/10.1080/09733159.2016.1244361

Gille, S. T., Sheen, K. L., Swart, S., & Thompson, A. F. (2022). Chapter 12—Mixing in the Southern Ocean. In M. Meredith & A. Naveira Garabato (Eds.), *Ocean Mixing* (pp. 301–327). Elsevier. https://doi.org/10.1016/B978-0-12-821512-8.00019-0

Global Ocean Biogeochemistry Analysis and Forecast. (n.d.). Retrieved September 25, 2024, from https://data.marine.copernicus.eu/product/GLOBAL_ANALYSISFORECAST_BGC_001_028/description

Guinotte, J. M., & Fabry, V. J. (2008). Ocean Acidification and Its Potential Effects on Marine Ecosystems. *Annals of the New York Academy of Sciences*, *1134*(1), 320–342. https://doi.org/10.1196/annals.1439.013

Ishii, M., Rodgers, K. B., Inoue, H. Y., Toyama, K., Sasano, D., Kosugi, N., Ono, H., Enyo, K., Nakano, T., Iudicone, D., Blanke, B., Aumont, O., & Feely, R. A. (2020). Ocean Acidification From Below in the Tropical Pacific. *Global Biogeochemical Cycles*, *34*(8). https://doi.org/10.1029/2019GB006368

Jiang, L.-Q., Carter, B. R., Feely, R. A., Lauvset, S. K., & Olsen, A. (2019). Surface ocean pH and buffer capacity: Past, present and future. *Sci Rep*, *9*(18624). https://doi.org/10.1038/s41598-019-55039-4

Joint Research Centre: Institute for Environment and Sustainability. (2011). *International reference life cycle data system (ILCD) handbook - General guide for life cycle assessment: Provisions and action steps*. Publications Office. https://doi.org/10.2788/33030

Kroeker, K. J., Kordas, R. L., Crim, R. N., & Singh, G. G. (2010). Meta-analysis reveals negative yet variable effects of ocean acidification on marine organisms. *Ecology Letters*, *13*(11), 1419–1434. https://doi.org/10.1111/j.1461-0248.2010.01518.x

Mostofa, K. M. G., Liu, C.-Q., Zhai, W., Minella, M., Vione, D., Gao, K., Minakata, D., Arakaki, T., Yoshioka, T., Hayakawa, K., Konohira, E., Tanoue, E., Akhand, A., Chanda, A., Wang, B., & Sakugawa, H. (2016). Reviews and Syntheses: Ocean acidification and its potential impacts

on marine ecosystems. *Biogeosciences*, *13*(6), 1767–1786. https://doi.org/10.5194/bg-13-1767-2016

Oginah, S. A. (2023). *Integrated risk assessment: From exposure through AOPs to ecosystem services*. Technical University of Denmark.

Owsianiak, M., Hauschild, M. Z., Posthuma, L., Saouter, E., Vijver, M. G., Backhaus, T., Douziech, M., Schlekat, T., & Fantke, P. (2023). Ecotoxicity characterization of chemicals: Global recommendations and implementation in USEtox. *Chemosphere*, *310*, 136807. https://doi.org/10.1016/j.chemosphere.2022.136807

Pansch, C., Schaub, I., Havenhand, J., & Wahl, M. (2014). Habitat traits and food availability determine the response of marine invertebrates to ocean acidification. *Global Change Biology*, *20*(3), 765–777. https://doi.org/10.1111/gcb.12478

PubChem. (n.d.). *Carbon Dioxide*. Retrieved September 26, 2024, from https://pubchem.ncbi.nlm.nih.gov/compound/280

R Core Team. (2024). *_R: A Language and Environment for Statistical Computing_* [Computer software]. R Foundation for Statistical Computing.

Radford, C. A., Collins, S. P., Munday, P. L., & Parsons, D. (2021). Ocean acidification effects on fish hearing. *Proceedings of the Royal Society B*, *288*(20202754). https://doi.org/10.1098/rspb.2020.2754

Rohli, R., Joyner, T., Reynolds, S., Shaw, C., & Vázquez, J. (2015). Globally Extended Kppen–Geiger climate classification and temporal shifts in terrestrial climatic types. *Physical Geography*, *36*, 142–157. https://doi.org/10.1080/02723646.2015.1016382

Scherer, L., Gürdal, İ., & van Bodegom, P. M. (2022). Characterization factors for ocean acidification impacts on marine biodiversity. *Journal of Industrial Ecology*, *26*(6), 2069–2079. https://doi.org/10.1111/jiec.13274

Silva, A. N., Purdie, D. A., Bates, N. R., & Tyrrell, T. (2024). Investigating Labrador Sea's persistent surface O2 anomaly using observations and biogeochemical model results. *Journal of Marine Systems*, *245*, 103996. https://doi.org/10.1016/j.jmarsys.2024.103996

Spalding, M. D., Fox, H. E., Allen, G. R., Davidson, N., Ferdaña, Z. A., Finlayson, M., Halpern, B. S., Jorge, M. A., Lombana, A., Lourie, S. A., Martin, K. D., McManus, E., Molnar, J., Recchia, C. A., & Robertson, J. (2007). Marine Ecoregions of the World: A Bioregionalization of Coastal

and Shelf Areas. *BioScience*, *57*(7), 573–583. https://doi.org/10.1641/B570707

van Vuuren, D. P., Edmonds, J., Kainuma, M., Riahi, K., Thomson, A., Hibbard, K., Hurtt, G. C., Kram, T., Krey, V., Lamarque, J.-F., Masui, T., Meinshausen, M., Nakicenovic, N., Smith, S. J., & Rose, S. K. (2011). The representative concentration pathways: An overview. *Climatic Change*, *109*(1), 5. https://doi.org/10.1007/s10584-011-0148-z

Vargas, C. A., Lagos, N. A., Lardies, M. A., Duarte, C., Manríquez, P. H., Aguilera, V. M., Broitman, B., Widdicombe, S., & Dupont, S. (2017). Species-specific responses to ocean acidification should account for local adaptation and adaptive plasticity. *Nature Ecology & Evolution*, *1*(4), 0084. https://doi.org/10.1038/s41559-017-0084

Woods, J. S., Veltman, K., Huijbregts, M. A. J., Verones, F., & Hertwich, E. G. (2016). Towards a meaningful assessment of marine ecological impacts in life cycle assessment (LCA). *Environment International*, *89–90*, 48–61. https://doi.org/10.1016/j.envint.2015.12.033

7 APPENDIX

Section 1: References for packages used in R

(1) Hijmans, R. terra: Spatial Data Analysis; R package version 1.8-55, 2025. https://rspatial.org/.
(2) Wickham, H. ggplot2: Elegant Graphics for Data Analysis; Springer-Verlag: New York, 2016.
(3) Wickham, H.; François, R.; Henry, L.; Müller, K.; Vaughan, D. dplyr: A Grammar of Data Manipulation; R package version 1.1.4, 2025. https://dplyr.tidyverse.org.
(4) Pebesma, E.; Bivand, R. Spatial Data Science: With Applications in R; Chapman and Hall/CRC: 2023. https://doi.org/10.1201/9780429459016.
(5) Schauberger, P.; Walker, A. openxlsx: Read, Write and Edit xlsx Files; R package version 4.2.8, 2025. https://github.com/ycphs/openxlsx; https://ycphs.github.io/openxlsx/index.html.
(6) Wickham, H.; Bryan, J. readxl: Read Excel Files; R package version 1.4.5, 2025. https://github.com/tidyverse/readxl; https://readxl.tidyverse.org.
(7) Pierce, D. ncdf4: Interface to Unidata netCDF (Version 4 or Earlier) Format Data Files; R package version 1.24, 2025. https://CRAN.R-project.org/package=ncdf4.

Table S1: Version information for packages used in Python

Package	**Version**
xarray	2024.9.0
gdal	3.9.3
netCDF4	1.7.2
rasterio	1.4.1
matplotlib	3.9.2
rioxarray	0.19.0
numpy	2.1.2

Section 2: References for studies used to calculate pH_{50} and pH_{10} for use in SSD curves

(1) Cripps, G.; Lindeque, P.; Flynn, K. J. Have We Been Underestimating the Effects of Ocean Acidification in Zooplankton? Global Change Biology 2014, 20 (11), 3377–3385. https://doi.org/10.1111/gcb.12582.

(2) Gazeau, F.; Quiblier, C.; Jansen, J. M.; Gattuso, J.-P.; Middelburg, J. J.; Heip, C. H. R. Impact of Elevated CO2 on Shellfish Calcification. Geophysical Research Letters 2007, 34 (7). https://doi.org/10.1029/2006GL028554.

(3) Tegomo, F. A.; Zhong, Z.; Njomoue, A. P.; Okon, S. U.; Ullah, S.; Gray, N. A.; Chen, K.; Sun, Y.; Xiao, J.; Wang, L.; Ye, Y.; Huang, H.; Shao, Q. Experimental Studies on the Impact of the Projected Ocean Acidification on Fish Survival, Health, Growth, and Meat Quality; Black Sea Bream (Acanthopagrus Schlegelii), Physiological and Histological Studies. Animals 2021, 11 (11), 3119. https://doi.org/10.3390/ani11113119.

(4) Crim, R. N.; Sunday, J. M.; Harley, C. D. G. Elevated Seawater CO2 Concentrations Impair Larval Development and Reduce Larval Survival in Endangered Northern Abalone (Haliotis

Kamtschatkana). Journal of Experimental Marine Biology and Ecology 2011, 400 (1), 272–277. https://doi.org/10.1016/j.jembe.2011.02.002.

(5) Inoue, M.; Suwa, R.; Suzuki, A.; Sakai, K.; Kawahata, H. Effects of Seawater pH on Growth and Skeletal U/Ca Ratios of Acropora Digitifera Coral Polyps. Geophysical Research Letters 2011, 38 (12). https://doi.org/10.1029/2011GL047786.

(6) Gonzalez-Bernat, M. J.; Lamare, M.; Barker, M. Effects of Reduced Seawater pH on Fertilisation, Embryogenesis and Larval Development in the Antarctic Seastar Odontaster Validus. Polar Biol 2013, 36 (2), 235–247. https://doi.org/10.1007/s00300-012-1255-7.

(7) Kurihara, H.; Shimode, S.; Shirayama, Y. Effects of Raised CO2 Concentration on the Egg Production Rate and Early Development of Two Marine Copepods (Acartia Steueri and Acartia Erythraea). Marine Pollution Bulletin 2004, 49 (9), 721–727. https://doi.org/10.1016/j.marpolbul.2004.05.005.

(8) Faria, A. M.; Filipe, S.; Lopes, A. F.; Oliveira, A. P.; Gonçalves, E. J.; Ribeiro, L. Effects of High pCO2 on Early Life Development of Pelagic Spawning Marine Fish. Mar. Freshwater Res. 2017, 68 (11), 2106–2114. https://doi.org/10.1071/MF16385.

(9) Renegar, D. A.; Riegl, B. M. Effect of Nutrient Enrichment and Elevated CO2 Partial Pressure on Growth Rate of Atlantic Scleractinian Coral Acropora Cervicornis. Marine Ecology Progress Series 2005, 293, 69–76. https://doi.org/10.3354/meps293069.

(10) Comeau, S.; Cornwall, C. E.; McCulloch, M. T. Decoupling between the Response of Coral Calcifying Fluid pH and Calcification to Ocean Acidification. Sci Rep 2017, 7 (1), 7573. https://doi.org/10.1038/s41598-017-08003-z.

(11) Sganga, D. E.; Dahlke, F. T.; Sørensen, S. R.; Butts, I. A. E.; Tomkiewicz, J.; Mazurais, D.; Servili, A.; Bertolini, F.; Politis, S. N. CO2 Induced Seawater Acidification Impacts Survival and Development of European Eel Embryos. PLOS ONE 2022, 17 (4), e0267228. https://doi.org/10.1371/journal.pone.0267228.

(12) Collard, M.; Eeckhaut, I.; Dehairs, F.; Dubois, P. Acid-Base Physiology Response to Ocean Acidification of Two Ecologically and Economically Important Holothuroids from Contrasting Habitats, Holothuria Scabra and Holothuria Parva. Environ Sci Pollut Res 2014, 21 (23), 13602–13614. https://doi.org/10.1007/s11356-014-3259-z.

(13) Small, D.; Calosi, P.; White, D.; Spicer, J. I.; Widdicombe, S. Impact of Medium-Term Exposure to CO2 Enriched Seawater on the Physiological Functions of the Velvet Swimming Crab Necora Puber. Aquatic Biology 2010, 10 (1), 11–21. https://doi.org/10.3354/ab00266.

(14) Appelhans, Y.; Thomsen, J.; Opitz, S.; Pansch, C.; Melzner, F.; Wahl, M. Juvenile Sea Stars Exposed to Acidification Decrease Feeding and Growth with No Acclimation Potential. Mar. Ecol. Prog. Ser. 2014, 509, 227–239. https://doi.org/10.3354/meps10884.

(15) Kamya, P. Z.; Dworjanyn, S. A.; Hardy, N.; Mos, B.; Uthicke, S.; Byrne, M. Larvae of the Coral Eating Crown-of-Thorns Starfish, Acanthaster Planci in a Warmer-High CO2 Ocean. Global Change Biology 2014, 20 (11), 3365–3376. https://doi.org/10.1111/gcb.12530.

(16) Zlatkin, R. L.; Heuer, R. M. Ocean Acidification Affects Acid–Base Physiology and Behaviour in a Model Invertebrate, the California Sea Hare (Aplysia Californica). Royal Society Open

Science 2019, 6 (10), 191041. https://doi.org/10.1098/rsos.191041.

(17) Munday, P. L.; Dixson, D. L.; Donelson, J. M.; Jones, G. P.; Pratchett, M. S.; Devitsina, G. V.; Døving, K. B. Ocean Acidification Impairs Olfactory Discrimination and Homing Ability of a Marine Fish. Proceedings of the National Academy of Sciences 2009, 106 (6), 1848–1852. https://doi.org/10.1073/pnas.0809996106.

(18) Stumpp, M.; Trübenbach, K.; Brennecke, D.; Hu, M. Y.; Melzner, F. Resource Allocation and Extracellular Acid–Base Status in the Sea Urchin Strongylocentrotus Droebachiensis in Response to CO2 Induced Seawater Acidification. Aquatic Toxicology 2012, 110–111, 194–207. https://doi.org/10.1016/j.aquatox.2011.12.020.

(19) Comeau, S.; Jeffree, R.; Teyssié, J.-L.; Gattuso, J.-P. Response of the Arctic Pteropod Limacina Helicina to Projected Future Environmental Conditions. PLOS ONE 2010, 5 (6), e11362. https://doi.org/10.1371/journal.pone.0011362.

(20) Frommel, A. Y.; Maneja, R.; Lowe, D.; Malzahn, A. M.; Geffen, A. J.; Folkvord, A.; Piatkowski, U.; Reusch, T. B. H.; Clemmesen, C. Severe Tissue Damage in Atlantic Cod Larvae under Increasing Ocean Acidification. Nature Clim Change 2012, 2 (1), 42–46. https://doi.org/10.1038/nclimate1324.

(21) Okazaki, R. R.; Towle, E. K.; van Hooidonk, R.; Mor, C.; Winter, R. N.; Piggot, A. M.; Cunning, R.; Baker, A. C.; Klaus, J. S.; Swart, P. K.; Langdon, C. Species-Specific Responses to Climate Change and Community Composition Determine Future Calcification Rates of Florida Keys Reefs. Global Change Biology 2017, 23 (3), 1023–1035. https://doi.org/10.1111/gcb.13481.

(22) Wisshak, M.; Schönberg, C. H. L.; Form, A.; Freiwald, A. Sponge Bioerosion Accelerated by Ocean Acidification across Species and Latitudes? Helgol Mar Res 2014, 68 (2), 253–262. https://doi.org/10.1007/s10152-014-0385-4.

(23) Talmage, S. C.; Gobler, C. J. The Effects of Elevated Carbon Dioxide Concentrations on the Metamorphosis, Size, and Survival of Larval Hard Clams (Mercenaria Mercenaria), Bay Scallops (Argopecten Irradians), and Eastern Oysters (Crassostrea Virginica). Limnology and Oceanography 2009, 54 (6), 2072–2080. https://doi.org/10.4319/lo.2009.54.6.2072.

*Table S2: Fate factor values for CO_2, CH_4, and CO [Pa*yr/kg] per marine ecoregion*

Marine ecoregion	CO_2	CH_4	CO
Adriatic Sea	3.05E-12	2.55E-12	2.66E-12
Aegean Sea	3.05E-12	2.54E-12	2.65E-12
Agulhas Bank	2.87E-12	2.39E-12	2.50E-12
Alboran Sea	3.15E-12	2.63E-12	2.74E-12
Aleutian Islands	4.72E-12	3.94E-12	4.11E-12
Amazonia	3.69E-12	3.08E-12	3.21E-12
Amsterdam-St Paul	3.40E-12	2.84E-12	2.96E-12
Amundsen/Bellingshausen Sea	4.32E-12	3.61E-12	3.77E-12
Andaman and Nicobar Islands	3.19E-12	2.66E-12	2.77E-12

Andaman Sea Coral Coast	3.21E-12	2.68E-12	2.79E-12
Angolan	3.42E-12	2.85E-12	2.98E-12
Antarctic Peninsula	4.20E-12	3.50E-12	3.66E-12
Arabian (Persian) Gulf	3.57E-12	2.98E-12	3.11E-12
Arafura Sea	3.26E-12	2.72E-12	2.84E-12
Araucanian	3.86E-12	3.22E-12	3.36E-12
Arnhem Coast to Gulf of Carpenteria	3.30E-12	2.75E-12	2.87E-12
Auckland Island	4.01E-12	3.35E-12	3.49E-12
Azores Canaries Madeira	3.20E-12	2.67E-12	2.79E-12
Baffin Bay - Davis Strait	3.99E-12	3.32E-12	3.47E-12
Bahamian	2.86E-12	2.39E-12	2.49E-12
Baltic Sea	3.36E-12	2.80E-12	2.92E-12
Banda Sea	3.35E-12	2.79E-12	2.92E-12
Bassian	3.47E-12	2.89E-12	3.02E-12
Beaufort Sea - continental coast and shelf	5.48E-12	4.57E-12	4.77E-12
Beaufort-Amundsen-Viscount Melville-Queen Maud	4.96E-12	4.14E-12	4.32E-12
Bermuda	2.93E-12	2.45E-12	2.55E-12
Bight of Sofala/Swamp Coast	3.08E-12	2.57E-12	2.68E-12
Bismarck Sea	3.50E-12	2.92E-12	3.05E-12
Black Sea	2.50E-12	2.09E-12	2.18E-12
Bonaparte Coast	3.34E-12	2.79E-12	2.91E-12
Bounty and Antipodes Islands	3.89E-12	3.24E-12	3.39E-12
Bouvet Island	4.71E-12	3.93E-12	4.10E-12
Campbell Island	4.15E-12	3.46E-12	3.61E-12
Cape Howe	3.00E-12	2.50E-12	2.61E-12
Cape Verde	3.11E-12	2.59E-12	2.71E-12
Cargados Carajos/Tromelin Island	3.16E-12	2.64E-12	2.76E-12
Carolinian	2.87E-12	2.39E-12	2.50E-12
Celtic Seas	3.45E-12	2.88E-12	3.01E-12
Central and Southern Great Barrier Reef	2.89E-12	2.41E-12	2.52E-12
Central Chile	3.82E-12	3.18E-12	3.32E-12
Central Kuroshio Current	2.91E-12	2.43E-12	2.54E-12
Central New Zealand	3.22E-12	2.69E-12	2.81E-12
Central Peru	4.62E-12	3.85E-12	4.02E-12
Central Somali Coast	3.20E-12	2.67E-12	2.79E-12
Chagos	3.17E-12	2.64E-12	2.76E-12
Channels and Fjords of Southern Chile	4.42E-12	3.68E-12	3.85E-12

Chatham Island	3.30E-12	2.76E-12	2.88E-12
Chiapas-Nicaragua	3.45E-12	2.88E-12	3.01E-12
Chiloense	4.24E-12	3.53E-12	3.69E-12
Chukchi Sea	4.03E-12	3.36E-12	3.51E-12
Clipperton	3.30E-12	2.76E-12	2.88E-12
Cocos Islands	3.55E-12	2.96E-12	3.09E-12
Cocos-Keeling/Christmas Island	3.15E-12	2.63E-12	2.75E-12
Coral Sea	2.93E-12	2.44E-12	2.55E-12
Cortezian	4.17E-12	3.48E-12	3.63E-12
Crozet Islands	4.32E-12	3.60E-12	3.76E-12
Delagoa	2.91E-12	2.43E-12	2.54E-12
East African Coral Coast	3.15E-12	2.62E-12	2.74E-12
East Antarctic Dronning Maud Land	4.67E-12	3.90E-12	4.07E-12
East Antarctic Enderby Land	4.85E-12	4.05E-12	4.23E-12
East Antarctic Wilkes Land	4.64E-12	3.87E-12	4.04E-12
East Caroline Islands	3.24E-12	2.70E-12	2.82E-12
East China Sea	3.05E-12	2.54E-12	2.65E-12
East Greenland Shelf	3.67E-12	3.06E-12	3.20E-12
East Siberian Sea	5.76E-12	4.80E-12	5.01E-12
Easter Island	3.24E-12	2.70E-12	2.82E-12
Eastern Bering Sea	4.31E-12	3.59E-12	3.75E-12
Eastern Brazil	2.96E-12	2.47E-12	2.58E-12
Eastern Caribbean	2.91E-12	2.42E-12	2.53E-12
Eastern Galapagos Islands	4.03E-12	3.36E-12	3.51E-12
Eastern India	3.07E-12	2.56E-12	2.67E-12
Eastern Philippines	3.15E-12	2.63E-12	2.74E-12
Exmouth to Broome	3.22E-12	2.68E-12	2.80E-12
Faroe Plateau	3.72E-12	3.11E-12	3.24E-12
Fernando de Naronha and Atoll das Rocas	3.40E-12	2.83E-12	2.96E-12
Fiji Islands	2.82E-12	2.35E-12	2.46E-12
Floridian	2.89E-12	2.41E-12	2.52E-12
Gilbert/Ellis Islands	3.36E-12	2.81E-12	2.93E-12
Great Australian Bight	3.24E-12	2.70E-12	2.82E-12
Greater Antilles	2.97E-12	2.48E-12	2.59E-12
Guayaquil	4.09E-12	3.41E-12	3.56E-12
Guianan	3.23E-12	2.69E-12	2.81E-12
Gulf of Aden	3.42E-12	2.85E-12	2.98E-12
Gulf of Alaska	4.26E-12	3.55E-12	3.71E-12
Gulf of Guinea Central	3.08E-12	2.57E-12	2.68E-12
Gulf of Guinea Islands	3.10E-12	2.58E-12	2.70E-12
Gulf of Guinea South	3.41E-12	2.85E-12	2.97E-12
Gulf of Guinea Upwelling	3.16E-12	2.64E-12	2.76E-12

Gulf of Guinea West	3.08E-12	2.57E-12	2.69E-12
Gulf of Maine/Bay of Fundy	4.11E-12	3.43E-12	3.58E-12
Gulf of Oman	3.41E-12	2.84E-12	2.97E-12
Gulf of Papua	3.36E-12	2.80E-12	2.93E-12
Gulf of St. Lawrence - Eastern Scotian Shelf	4.99E-12	4.16E-12	4.35E-12
Gulf of Thailand	3.36E-12	2.80E-12	2.92E-12
Gulf of Tonkin	3.27E-12	2.73E-12	2.85E-12
Halmahera	3.39E-12	2.83E-12	2.95E-12
Hawaii	3.07E-12	2.56E-12	2.67E-12
Heard and Macdonald Islands	4.57E-12	3.81E-12	3.98E-12
High Arctic Archipelago	4.72E-12	3.93E-12	4.11E-12
Houtman	2.93E-12	2.44E-12	2.55E-12
Hudson Complex	4.03E-12	3.36E-12	3.51E-12
Humboldtian	4.13E-12	3.44E-12	3.60E-12
Ionian Sea	3.18E-12	2.66E-12	2.77E-12
Juan Fernandez and Desventuradas	3.70E-12	3.08E-12	3.22E-12
Kamchatka Shelf and Coast	4.41E-12	3.68E-12	3.85E-12
Kara Sea	4.41E-12	3.68E-12	3.84E-12
Kerguelen Islands	4.43E-12	3.69E-12	3.86E-12
Kermadec Island	2.99E-12	2.49E-12	2.60E-12
Lancaster Sound	4.26E-12	3.55E-12	3.71E-12
Laptev Sea	5.72E-12	4.77E-12	4.98E-12
Leeuwin	3.13E-12	2.61E-12	2.73E-12
Lesser Sunda	3.39E-12	2.83E-12	2.95E-12
Levantine Sea	3.04E-12	2.54E-12	2.65E-12
Line Islands	3.62E-12	3.02E-12	3.16E-12
Lord Howe and Norfolk Islands	2.91E-12	2.43E-12	2.53E-12
Macquarie Island	4.33E-12	3.61E-12	3.77E-12
Magdalena Transition	3.87E-12	3.23E-12	3.37E-12
Malacca Strait	3.27E-12	2.73E-12	2.85E-12
Maldives	3.11E-12	2.59E-12	2.71E-12
Malvinas/Falklands	3.98E-12	3.32E-12	3.47E-12
Manning-Hawkesbury	2.87E-12	2.39E-12	2.50E-12
Mariana Islands	3.00E-12	2.50E-12	2.61E-12
Marquesas	3.23E-12	2.69E-12	2.81E-12
Marshall Islands	3.08E-12	2.57E-12	2.68E-12
Mascarene Islands	3.02E-12	2.52E-12	2.63E-12
Mexican Tropical Pacific	3.49E-12	2.91E-12	3.04E-12
Namaqua	2.94E-12	2.45E-12	2.56E-12
Namib	3.62E-12	3.02E-12	3.15E-12
Natal	2.90E-12	2.42E-12	2.53E-12

New Caledonia	2.91E-12	2.43E-12	2.53E-12
Nicoya	3.65E-12	3.05E-12	3.18E-12
Ningaloo	3.04E-12	2.53E-12	2.64E-12
North American Pacific Fijordland	4.21E-12	3.51E-12	3.67E-12
North and East Barents Sea	3.21E-12	2.67E-12	2.79E-12
North and East Iceland	3.72E-12	3.11E-12	3.24E-12
North Greenland	3.87E-12	3.23E-12	3.37E-12
North Patagonian Gulfs	3.58E-12	2.99E-12	3.12E-12
North Sea	3.64E-12	3.04E-12	3.17E-12
Northeast Sulawesi	3.18E-12	2.65E-12	2.77E-12
Northeastern Brazil	3.16E-12	2.64E-12	2.75E-12
Northeastern Honshu	3.18E-12	2.65E-12	2.77E-12
Northeastern New Zealand	3.05E-12	2.55E-12	2.66E-12
Northern and Central Red Sea	3.51E-12	2.93E-12	3.06E-12
Northern Bay of Bengal	3.22E-12	2.68E-12	2.80E-12
Northern California	3.94E-12	3.29E-12	3.43E-12
Northern Galapagos Islands	3.45E-12	2.87E-12	3.00E-12
Northern Grand Banks - Southern Labrador	3.93E-12	3.28E-12	3.42E-12
Northern Gulf of Mexico	2.97E-12	2.48E-12	2.59E-12
Northern Labrador	3.66E-12	3.06E-12	3.19E-12
Northern Monsoon Current Coast	3.15E-12	2.63E-12	2.75E-12
Northern Norway and Finnmark	3.46E-12	2.88E-12	3.01E-12
Ogasawara Islands	2.98E-12	2.49E-12	2.60E-12
Oregon, Washington, Vancouver Coast and Shelf	3.88E-12	3.24E-12	3.38E-12
Oyashio Current	4.24E-12	3.53E-12	3.69E-12
Palawan/North Borneo	3.27E-12	2.73E-12	2.85E-12
Panama Bight	3.33E-12	2.78E-12	2.90E-12
Papua	3.53E-12	2.94E-12	3.07E-12
Patagonian Shelf	3.79E-12	3.16E-12	3.30E-12
Peter the First Island	4.52E-12	3.77E-12	3.94E-12
Phoenix/Tokelau/Northern Cook Islands	3.18E-12	2.65E-12	2.77E-12
Prince Edward Islands	4.22E-12	3.52E-12	3.68E-12
Puget Trough/Georgia Basin	4.10E-12	3.42E-12	3.57E-12
Rapa-Pitcairn	2.97E-12	2.48E-12	2.59E-12
Revillagigedos	3.41E-12	2.85E-12	2.97E-12
Rio de la Plata	3.21E-12	2.68E-12	2.80E-12
Rio Grande	3.07E-12	2.56E-12	2.67E-12
Ross Sea	4.16E-12	3.47E-12	3.62E-12
Saharan Upwelling	3.16E-12	2.64E-12	2.75E-12

Sahelian Upwelling	3.35E-12	2.79E-12	2.91E-12
Samoa Islands	2.83E-12	2.36E-12	2.46E-12
Sao Pedro and Sao Paulo Islands	3.34E-12	2.78E-12	2.91E-12
Scotian Shelf	4.26E-12	3.55E-12	3.71E-12
Sea of Japan/East Sea	3.16E-12	2.64E-12	2.76E-12
Sea of Okhotsk	4.03E-12	3.36E-12	3.51E-12
Seychelles	3.20E-12	2.67E-12	2.79E-12
Shark Bay	2.93E-12	2.45E-12	2.55E-12
Snares Island	3.77E-12	3.14E-12	3.28E-12
Society Islands	2.82E-12	2.35E-12	2.46E-12
Solomon Archipelago	3.23E-12	2.69E-12	2.81E-12
Solomon Sea	3.09E-12	2.58E-12	2.69E-12
South and West Iceland	3.77E-12	3.15E-12	3.29E-12
South Australian Gulfs	3.38E-12	2.82E-12	2.95E-12
South China Sea Oceanic Islands	3.28E-12	2.73E-12	2.85E-12
South European Atlantic Shelf	3.27E-12	2.73E-12	2.85E-12
South Georgia	4.68E-12	3.91E-12	4.08E-12
South India and Sri Lanka	3.17E-12	2.64E-12	2.76E-12
South Kuroshio	2.99E-12	2.49E-12	2.61E-12
South New Zealand	3.63E-12	3.03E-12	3.16E-12
South Orkney Islands	4.65E-12	3.88E-12	4.05E-12
South Sandwich Islands	4.62E-12	3.85E-12	4.02E-12
South Shetland Islands	4.72E-12	3.94E-12	4.11E-12
Southeast Madagascar	2.94E-12	2.45E-12	2.56E-12
Southeast Papua New Guinea	3.01E-12	2.51E-12	2.62E-12
Southeastern Brazil	2.99E-12	2.50E-12	2.61E-12
Southern California Bight	3.86E-12	3.22E-12	3.36E-12
Southern Caribbean	3.12E-12	2.60E-12	2.71E-12
Southern China	3.15E-12	2.63E-12	2.74E-12
Southern Cook/Austral Islands	2.85E-12	2.37E-12	2.48E-12
Southern Grand Banks - South Newfoundland	4.32E-12	3.60E-12	3.76E-12
Southern Gulf of Mexico	2.92E-12	2.44E-12	2.54E-12
Southern Java	3.27E-12	2.73E-12	2.85E-12
Southern Norway	3.60E-12	3.00E-12	3.14E-12
Southern Red Sea	4.18E-12	3.48E-12	3.64E-12
Southern Vietnam	3.33E-12	2.78E-12	2.90E-12
Southwestern Caribbean	3.07E-12	2.56E-12	2.67E-12
St. Helena and Ascension Islands	3.18E-12	2.65E-12	2.77E-12
Sulawesi Sea/Makassar Strait	3.32E-12	2.77E-12	2.89E-12
Sunda Shelf/Java Sea	3.45E-12	2.88E-12	3.01E-12

Three Kings-North Cape	2.98E-12	2.48E-12	2.59E-12
Tonga Islands	2.78E-12	2.32E-12	2.42E-12
Torres Strait Northern Great Barrier Reef	3.06E-12	2.55E-12	2.66E-12
Trindade and Martin Vaz Islands	3.07E-12	2.56E-12	2.67E-12
Tristan Gough	3.61E-12	3.02E-12	3.15E-12
Tuamotus	2.88E-12	2.40E-12	2.51E-12
Tunisian Plateau/Gulf of Sidra	3.15E-12	2.63E-12	2.74E-12
Tweed-Moreton	2.85E-12	2.38E-12	2.48E-12
Uruguay-Buenos Aires Shelf	3.22E-12	2.68E-12	2.80E-12
Vanuatu	2.91E-12	2.43E-12	2.54E-12
Virginian	3.38E-12	2.82E-12	2.94E-12
Weddell Sea	3.55E-12	2.96E-12	3.09E-12
West Caroline Islands	3.28E-12	2.74E-12	2.86E-12
West Greenland Shelf	3.46E-12	2.89E-12	3.01E-12
Western and Northern Madagascar	3.07E-12	2.56E-12	2.67E-12
Western Arabian Sea	3.52E-12	2.94E-12	3.07E-12
Western Bassian	3.50E-12	2.92E-12	3.05E-12
Western Caribbean	3.00E-12	2.50E-12	2.61E-12
Western Galapagos Islands	4.28E-12	3.57E-12	3.73E-12
Western India	2.92E-12	2.43E-12	2.54E-12
Western Mediterranean	3.27E-12	2.72E-12	2.84E-12
Western Sumatra	3.28E-12	2.73E-12	2.85E-12
White Sea	3.59E-12	3.00E-12	3.13E-12
Yellow Sea	3.54E-12	2.96E-12	3.09E-12

*Table S3: Fate factor values for CO_2, CH_4, and CO [Pa*yr/kg] per FAO major fishing area*

FAO major fishing area	**CO_2**	**CH_4**	**CO**
18	4.41E-12	3.68E-12	3.84E-12
21	3.42E-12	2.85E-12	2.98E-12
27	3.52E-12	2.94E-12	3.07E-12
31	2.92E-12	2.43E-12	2.54E-12
34	3.10E-12	2.59E-12	2.70E-12
41	3.42E-12	2.86E-12	2.98E-12
47	3.47E-12	2.90E-12	3.03E-12
48	4.49E-12	3.74E-12	3.91E-12
51	3.17E-12	2.64E-12	2.76E-12
57	3.54E-12	2.96E-12	3.09E-12
58	4.70E-12	3.92E-12	4.09E-12
61	3.49E-12	2.91E-12	3.04E-12
67	4.16E-12	3.47E-12	3.62E-12
71	3.14E-12	2.62E-12	2.73E-12
77	3.38E-12	2.82E-12	2.94E-12

81	3.68E-12	3.07E-12	3.21E-12
87	3.84E-12	3.20E-12	3.34E-12
88	4.62E-12	3.85E-12	4.02E-12

Table S4: Fate sensitivity factor values [pH/Pa] per marine ecoregions

Marine ecoregion	FSF
Adriatic Sea	-1.15E-02
Aegean Sea	-1.51E-02
Agulhas Bank	-1.03E-02
Alboran Sea	-1.06E-02
Aleutian Islands	-9.08E-03
Amazonia	-9.12E-03
Amsterdam-St Paul	-8.27E-03
Amundsen/Bellingshausen Sea	-1.19E-02
Andaman and Nicobar Islands	-9.55E-03
Andaman Sea Coral Coast	-8.52E-03
Angolan	-7.40E-03
Antarctic Peninsula	-1.22E-02
Arabian (Persian) Gulf	-9.46E-03
Arafura Sea	-5.09E-03
Araucanian	-8.73E-03
Arnhem Coast to Gulf of Carpenteria	-6.58E-03
Auckland Island	-9.83E-03
Azores Canaries Madeira	-8.33E-03
Baffin Bay - Davis Strait	-1.15E-02
Bahamian	-1.30E-02
Baltic Sea	-1.52E-02
Banda Sea	-8.01E-03
Bassian	-9.67E-03
Beaufort Sea - continental coast and shelf	-6.72E-03
Beaufort-Amundsen-Viscount Melville-Queen Maud	-1.15E-02
Bermuda	-1.07E-02
Bight of Sofala/Swamp Coast	-5.13E-03
Bismarck Sea	-6.42E-03
Black Sea	-1.01E-02
Bonaparte Coast	-4.67E-03
Bounty and Antipodes Islands	-1.01E-02
Bouvet Island	-1.04E-02
Campbell Island	-1.02E-02
Cape Howe	-9.56E-03
Cape Verde	-8.97E-03
Cargados Carajos/Tromelin Island	-9.30E-03
Carolinian	-1.22E-02

Celtic Seas	-9.39E-03
Central and Southern Great Barrier Reef	-7.27E-03
Central Chile	-7.53E-03
Central Kuroshio Current	-1.18E-02
Central New Zealand	-9.85E-03
Central Peru	-6.99E-03
Central Somali Coast	-9.34E-03
Chagos	-6.52E-03
Channels and Fjords of Southern Chile	-8.64E-03
Chatham Island	-9.94E-03
Chiapas-Nicaragua	-7.25E-03
Chiloense	-8.91E-03
Chukchi Sea	-1.15E-02
Clipperton	-8.11E-03
Cocos Islands	-6.79E-03
Cocos-Keeling/Christmas Island	-7.61E-03
Coral Sea	-1.03E-02
Cortezian	-7.72E-03
Crozet Islands	-9.01E-03
Delagoa	-7.61E-03
East African Coral Coast	-5.66E-03
East Antarctic Dronning Maud Land	-1.06E-02
East Antarctic Enderby Land	-1.17E-02
East Antarctic Wilkes Land	-1.08E-02
East Caroline Islands	-8.03E-03
East China Sea	-8.72E-03
East Greenland Shelf	-9.89E-03
East Siberian Sea	-1.21E-02
Easter Island	-1.03E-02
Eastern Bering Sea	-9.12E-03
Eastern Brazil	-8.22E-03
Eastern Caribbean	-1.27E-02
Eastern Galapagos Islands	-6.29E-03
Eastern India	-1.20E-02
Eastern Philippines	-7.11E-03
Exmouth to Broome	-6.21E-03
Faroe Plateau	-8.30E-03
Fernando de Naronha and Atoll das Rocas	-8.48E-03
Fiji Islands	-1.25E-02
Floridian	-1.26E-02
Gilbert/Ellis Islands	-7.53E-03
Great Australian Bight	-8.76E-03
Greater Antilles	-1.08E-02

Guayaquil	-7.43E-03
Guianan	-5.56E-03
Gulf of Aden	-8.85E-03
Gulf of Alaska	-9.27E-03
Gulf of Guinea Central	-7.18E-03
Gulf of Guinea Islands	-7.14E-03
Gulf of Guinea South	-6.83E-03
Gulf of Guinea Upwelling	-8.61E-03
Gulf of Guinea West	-7.76E-03
Gulf of Maine/Bay of Fundy	-1.31E-02
Gulf of Oman	-8.23E-03
Gulf of Papua	-5.46E-03
Gulf of St. Lawrence - Eastern Scotian Shelf	-1.14E-02
Gulf of Thailand	-4.71E-03
Gulf of Tonkin	-1.19E-02
Halmahera	-7.45E-03
Hawaii	-1.06E-02
Heard and Macdonald Islands	-1.15E-02
High Arctic Archipelago	-1.12E-02
Houtman	-9.78E-03
Hudson Complex	-7.15E-03
Humboldtian	-7.17E-03
Ionian Sea	-9.66E-03
Juan Fernandez and Desventuradas	-7.99E-03
Kamchatka Shelf and Coast	-9.42E-03
Kara Sea	-9.80E-03
Kerguelen Islands	-1.03E-02
Kermadec Island	-7.90E-03
Lancaster Sound	-1.28E-02
Laptev Sea	-1.60E-02
Leeuwin	-1.01E-02
Lesser Sunda	-8.02E-03
Levantine Sea	-9.29E-03
Line Islands	-7.49E-03
Lord Howe and Norfolk Islands	-8.20E-03
Macquarie Island	-7.79E-03
Magdalena Transition	-8.49E-03
Malacca Strait	-5.91E-03
Maldives	-9.06E-03
Malvinas/Falklands	-9.80E-03
Manning-Hawkesbury	-9.30E-03
Mariana Islands	-1.04E-02
Marquesas	-8.93E-03
Marshall Islands	-8.79E-03
Mascarene Islands	-8.96E-03

Mexican Tropical Pacific	-7.93E-03
Namaqua	-9.79E-03
Namib	-8.14E-03
Natal	-9.65E-03
New Caledonia	-8.62E-03
Nicoya	-6.69E-03
Ningaloo	-1.05E-02
North American Pacific Fijordland	-8.79E-03
North and East Barents Sea	-1.03E-02
North and East Iceland	-9.68E-03
North Greenland	-1.20E-02
North Patagonian Gulfs	-9.67E-03
North Sea	-1.43E-02
Northeast Sulawesi	-8.00E-03
Northeastern Brazil	-1.05E-02
Northeastern Honshu	-1.13E-02
Northeastern New Zealand	-9.40E-03
Northern and Central Red Sea	-9.20E-03
Northern Bay of Bengal	-1.26E-02
Northern California	-8.27E-03
Northern Galapagos Islands	-7.65E-03
Northern Grand Banks - Southern Labrador	-9.60E-03
Northern Gulf of Mexico	-1.17E-02
Northern Labrador	-1.28E-02
Northern Monsoon Current Coast	-8.71E-03
Northern Norway and Finnmark	-1.07E-02
Ogasawara Islands	-1.07E-02
Oregon, Washington, Vancouver Coast and Shelf	-8.09E-03
Oyashio Current	-1.14E-02
Palawan/North Borneo	-6.42E-03
Panama Bight	-6.38E-03
Papua	-6.70E-03
Patagonian Shelf	-9.55E-03
Peter the First Island	-9.42E-03
Phoenix/Tokelau/Northern Cook Islands	-8.33E-03
Prince Edward Islands	-1.11E-02
Puget Trough/Georgia Basin	-1.24E-02
Rapa-Pitcairn	-1.01E-02
Revillagigedos	-7.63E-03
Rio de la Plata	-1.47E-04
Rio Grande	-9.02E-03
Ross Sea	-1.25E-02
Saharan Upwelling	-9.89E-03

Sahelian Upwelling	-8.73E-03
Samoa Islands	-9.52E-03
Sao Pedro and Sao Paulo Islands	-7.10E-03
Scotian Shelf	-1.27E-02
Sea of Japan/East Sea	-1.32E-02
Sea of Okhotsk	-1.13E-02
Seychelles	-8.25E-03
Shark Bay	-7.55E-03
Snares Island	-9.96E-03
Society Islands	-7.36E-03
Solomon Archipelago	-7.30E-03
Solomon Sea	-7.77E-03
South and West Iceland	-9.24E-03
South Australian Gulfs	-8.49E-03
South China Sea Oceanic Islands	-1.07E-02
South European Atlantic Shelf	-8.69E-03
South Georgia	-9.92E-03
South India and Sri Lanka	-9.88E-03
South Kuroshio	-1.11E-02
South New Zealand	-9.83E-03
South Orkney Islands	-1.10E-02
South Sandwich Islands	-1.06E-02
South Shetland Islands	-1.13E-02
Southeast Madagascar	-9.31E-03
Southeast Papua New Guinea	-5.64E-03
Southeastern Brazil	-7.88E-03
Southern California Bight	-8.68E-03
Southern Caribbean	-8.25E-03
Southern China	-1.28E-02
Southern Cook/Austral Islands	-8.57E-03
Southern Grand Banks - South Newfoundland	-1.25E-02
Southern Gulf of Mexico	-1.06E-02
Southern Java	-8.15E-03
Southern Norway	-1.01E-02
Southern Red Sea	-7.17E-03
Southern Vietnam	-9.15E-03
Southwestern Caribbean	-9.15E-03
St. Helena and Ascension Islands	-1.09E-02
Sulawesi Sea/Makassar Strait	-6.60E-03
Sunda Shelf/Java Sea	-7.98E-03
Three Kings-North Cape	-9.25E-03
Tonga Islands	-8.94E-03
Torres Strait Northern Great Barrier Reef	-8.47E-03

Trindade and Martin Vaz Islands	-9.76E-03
Tristan Gough	-8.07E-03
Tuamotus	-8.89E-03
Tunisian Plateau/Gulf of Sidra	-1.10E-02
Tweed-Moreton	-9.68E-03
Uruguay-Buenos Aires Shelf	-9.83E-03
Vanuatu	-1.00E-02
Virginian	-1.28E-02
Weddell Sea	-1.27E-02
West Caroline Islands	-8.19E-03
West Greenland Shelf	-9.69E-03
Western and Northern Madagascar	-7.73E-03
Western Arabian Sea	-7.93E-03
Western Bassian	-8.93E-03
Western Caribbean	-6.73E-03
Western Galapagos Islands	-6.63E-03
Western India	-1.01E-02
Western Mediterranean	-7.79E-03
Western Sumatra	-7.15E-03
White Sea	-7.08E-03
Yellow Sea	-1.28E-02
Adriatic Sea	-1.15E-02

Table S5: Fate sensitivity factor values [pH/Pa] per FAO major fishing areas

FAO major fishing area	**CO_2**
18	-1.08E-02
21	-4.45E-03
27	-7.68E-03
31	-8.93E-03
34	-7.00E-03
41	-8.88E-03
47	-8.77E-03
48	-5.96E-03
51	-1.10E-02
57	-9.57E-03
58	-7.69E-03
61	-1.01E-02
67	-5.94E-03
71	-7.15E-03
77	-7.05E-03
81	-1.06E-02
87	-7.65E-03
88	-4.58E-03

*Table S6: Midpoint characterization factor values for CO_2, CH_4, and CO [pH*yr/kg] per marine ecoregion*

Marine ecoregion	CO_2	CH_4	CO
Adriatic Sea	3.51E-14	2.92E-14	3.05E-14
Aegean Sea	4.61E-14	3.84E-14	4.01E-14
Agulhas Bank	2.94E-14	2.46E-14	2.56E-14
Alboran Sea	3.33E-14	2.78E-14	2.90E-14
Aleutian Islands	4.29E-14	3.57E-14	3.73E-14
Amazonia	3.36E-14	2.81E-14	2.93E-14
Amsterdam-St Paul	2.81E-14	2.35E-14	2.45E-14
Amundsen/Bellingshausen Sea	5.13E-14	4.28E-14	4.47E-14
Andaman and Nicobar Islands	3.04E-14	2.54E-14	2.65E-14
Andaman Sea Coral Coast	2.74E-14	2.28E-14	2.38E-14
Angolan	2.53E-14	2.11E-14	2.20E-14
Antarctic Peninsula	5.13E-14	4.28E-14	4.46E-14
Arabian (Persian) Gulf	3.38E-14	2.82E-14	2.94E-14
Arafura Sea	1.66E-14	1.39E-14	1.45E-14
Araucanian	3.37E-14	2.81E-14	2.94E-14
Arnhem Coast to Gulf of Carpenteria	2.17E-14	1.81E-14	1.89E-14
Auckland Island	3.95E-14	3.29E-14	3.44E-14
Azores Canaries Madeira	2.66E-14	2.22E-14	2.32E-14
Baffin Bay - Davis Strait	4.59E-14	3.83E-14	4.00E-14
Bahamian	3.72E-14	3.10E-14	3.24E-14
Baltic Sea	5.10E-14	4.25E-14	4.44E-14
Banda Sea	2.68E-14	2.24E-14	2.34E-14
Bassian	3.35E-14	2.80E-14	2.92E-14
Beaufort Sea - continental coast and shelf	3.68E-14	3.07E-14	3.20E-14
Beaufort-Amundsen-Viscount Melville-Queen Maud	5.73E-14	4.78E-14	4.99E-14
Bermuda	3.14E-14	2.62E-14	2.73E-14
Bight of Sofala/Swamp Coast	1.58E-14	1.32E-14	1.38E-14
Bismarck Sea	2.25E-14	1.87E-14	1.96E-14
Black Sea	2.52E-14	2.10E-14	2.19E-14
Bonaparte Coast	1.56E-14	1.30E-14	1.36E-14
Bounty and Antipodes Islands	3.91E-14	3.26E-14	3.40E-14
Bouvet Island	4.90E-14	4.08E-14	4.27E-14
Campbell Island	4.22E-14	3.52E-14	3.67E-14
Cape Howe	2.86E-14	2.39E-14	2.49E-14
Cape Verde	2.79E-14	2.33E-14	2.43E-14
Cargados Carajos/Tromelin Island	2.94E-14	2.45E-14	2.56E-14
Carolinian	3.49E-14	2.91E-14	3.04E-14
Celtic Seas	3.24E-14	2.70E-14	2.82E-14
Central and Southern Great Barrier Reef	2.10E-14	1.75E-14	1.83E-14
Central Chile	2.88E-14	2.40E-14	2.50E-14

Central Kuroshio Current	3.44E-14	2.87E-14	3.00E-14
Central New Zealand	3.18E-14	2.65E-14	2.77E-14
Central Peru	3.23E-14	2.69E-14	2.81E-14
Central Somali Coast	2.99E-14	2.49E-14	2.60E-14
Chagos	2.07E-14	1.72E-14	1.80E-14
Channels and Fjords of Southern Chile	3.82E-14	3.18E-14	3.32E-14
Chatham Island	3.28E-14	2.74E-14	2.86E-14
Chiapas-Nicaragua	2.50E-14	2.09E-14	2.18E-14
Chiloense	3.77E-14	3.15E-14	3.29E-14
Chukchi Sea	4.62E-14	3.85E-14	4.02E-14
Clipperton	2.68E-14	2.23E-14	2.33E-14
Cocos Islands	2.41E-14	2.01E-14	2.10E-14
Cocos-Keeling/Christmas Island	2.40E-14	2.00E-14	2.09E-14
Coral Sea	3.01E-14	2.51E-14	2.62E-14
Cortezian	3.22E-14	2.68E-14	2.80E-14
Crozet Islands	3.89E-14	3.25E-14	3.39E-14
Delagoa	2.22E-14	1.85E-14	1.93E-14
East African Coral Coast	1.78E-14	1.48E-14	1.55E-14
East Antarctic Dronning Maud Land	4.97E-14	4.15E-14	4.33E-14
East Antarctic Enderby Land	5.66E-14	4.72E-14	4.93E-14
East Antarctic Wilkes Land	5.02E-14	4.19E-14	4.37E-14
East Caroline Islands	2.60E-14	2.17E-14	2.27E-14
East China Sea	2.66E-14	2.22E-14	2.31E-14
East Greenland Shelf	3.63E-14	3.03E-14	3.16E-14
East Siberian Sea	6.94E-14	5.79E-14	6.04E-14
Easter Island	3.32E-14	2.77E-14	2.89E-14
Eastern Bering Sea	3.93E-14	3.28E-14	3.42E-14
Eastern Brazil	2.44E-14	2.03E-14	2.12E-14
Eastern Caribbean	3.70E-14	3.09E-14	3.23E-14
Eastern Galapagos Islands	2.53E-14	2.11E-14	2.21E-14
Eastern India	3.68E-14	3.07E-14	3.20E-14
Eastern Philippines	2.24E-14	1.87E-14	1.95E-14
Exmouth to Broome	2.00E-14	1.67E-14	1.74E-14
Faroe Plateau	3.09E-14	2.58E-14	2.69E-14
Fernando de Naronha and Atoll das Rocas	2.88E-14	2.40E-14	2.51E-14
Fiji Islands	3.52E-14	2.94E-14	3.07E-14
Floridian	3.65E-14	3.04E-14	3.18E-14
Gilbert/Ellis Islands	2.53E-14	2.11E-14	2.21E-14
Great Australian Bight	2.83E-14	2.36E-14	2.47E-14
Greater Antilles	3.22E-14	2.68E-14	2.80E-14
Guayaquil	3.04E-14	2.53E-14	2.65E-14
Guianan	1.80E-14	1.50E-14	1.56E-14
Gulf of Aden	3.03E-14	2.52E-14	2.63E-14

Gulf of Alaska	3.94E-14	3.29E-14	3.44E-14
Gulf of Guinea Central	2.21E-14	1.84E-14	1.93E-14
Gulf of Guinea Islands	2.21E-14	1.84E-14	1.92E-14
Gulf of Guinea South	2.33E-14	1.94E-14	2.03E-14
Gulf of Guinea Upwelling	2.72E-14	2.27E-14	2.37E-14
Gulf of Guinea West	2.39E-14	2.00E-14	2.08E-14
Gulf of Maine/Bay of Fundy	5.40E-14	4.50E-14	4.70E-14
Gulf of Oman	2.80E-14	2.34E-14	2.44E-14
Gulf of Papua	1.83E-14	1.53E-14	1.60E-14
Gulf of St. Lawrence - Eastern Scotian Shelf	5.69E-14	4.75E-14	4.96E-14
Gulf of Thailand	1.58E-14	1.32E-14	1.38E-14
Gulf of Tonkin	3.88E-14	3.24E-14	3.38E-14
Halmahera	2.52E-14	2.10E-14	2.20E-14
Hawaii	3.24E-14	2.70E-14	2.82E-14
Heard and Macdonald Islands	5.24E-14	4.37E-14	4.56E-14
High Arctic Archipelago	5.29E-14	4.42E-14	4.61E-14
Houtman	2.87E-14	2.39E-14	2.50E-14
Hudson Complex	2.88E-14	2.41E-14	2.51E-14
Humboldtian	2.96E-14	2.47E-14	2.58E-14
Ionian Sea	3.08E-14	2.57E-14	2.68E-14
Juan Fernandez and Desventuradas	2.95E-14	2.46E-14	2.57E-14
Kamchatka Shelf and Coast	4.16E-14	3.47E-14	3.62E-14
Kara Sea	4.32E-14	3.60E-14	3.76E-14
Kerguelen Islands	4.56E-14	3.80E-14	3.97E-14
Kermadec Island	2.36E-14	1.97E-14	2.06E-14
Lancaster Sound	5.43E-14	4.53E-14	4.73E-14
Laptev Sea	9.16E-14	7.64E-14	7.98E-14
Leeuwin	3.17E-14	2.65E-14	2.77E-14
Lesser Sunda	2.72E-14	2.27E-14	2.37E-14
Levantine Sea	2.83E-14	2.36E-14	2.46E-14
Line Islands	2.71E-14	2.26E-14	2.36E-14
Lord Howe and Norfolk Islands	2.39E-14	1.99E-14	2.08E-14
Macquarie Island	3.37E-14	2.81E-14	2.94E-14
Magdalena Transition	3.28E-14	2.74E-14	2.86E-14
Malacca Strait	1.93E-14	1.61E-14	1.68E-14
Maldives	2.82E-14	2.35E-14	2.45E-14
Malvinas/Falklands	3.90E-14	3.25E-14	3.40E-14
Manning-Hawkesbury	2.67E-14	2.23E-14	2.33E-14
Mariana Islands	3.13E-14	2.61E-14	2.72E-14
Marquesas	2.88E-14	2.40E-14	2.51E-14
Marshall Islands	2.71E-14	2.26E-14	2.36E-14
Mascarene Islands	2.70E-14	2.25E-14	2.35E-14
Mexican Tropical Pacific	2.77E-14	2.31E-14	2.41E-14
Namaqua	2.88E-14	2.40E-14	2.50E-14
Namib	2.95E-14	2.46E-14	2.57E-14

Natal	2.80E-14	2.33E-14	2.44E-14
New Caledonia	2.51E-14	2.09E-14	2.18E-14
Nicoya	2.44E-14	2.04E-14	2.13E-14
Ningaloo	3.19E-14	2.66E-14	2.78E-14
North American Pacific Fijordland	3.70E-14	3.08E-14	3.22E-14
North and East Barents Sea	3.29E-14	2.74E-14	2.86E-14
North and East Iceland	3.60E-14	3.01E-14	3.14E-14
North Greenland	4.66E-14	3.88E-14	4.05E-14
North Patagonian Gulfs	3.46E-14	2.89E-14	3.02E-14
North Sea	5.21E-14	4.35E-14	4.54E-14
Northeast Sulawesi	2.54E-14	2.12E-14	2.22E-14
Northeastern Brazil	3.30E-14	2.75E-14	2.88E-14
Northeastern Honshu	3.58E-14	2.98E-14	3.12E-14
Northeastern New Zealand	2.87E-14	2.40E-14	2.50E-14
Northern and Central Red Sea	3.23E-14	2.69E-14	2.81E-14
Northern Bay of Bengal	4.04E-14	3.37E-14	3.52E-14
Northern California	3.26E-14	2.72E-14	2.84E-14
Northern Galapagos Islands	2.63E-14	2.20E-14	2.30E-14
Northern Grand Banks - Southern Labrador	3.77E-14	3.14E-14	3.28E-14
Northern Gulf of Mexico	3.49E-14	2.91E-14	3.04E-14
Northern Labrador	4.69E-14	3.91E-14	4.09E-14
Northern Monsoon Current Coast	2.75E-14	2.29E-14	2.39E-14
Northern Norway and Finnmark	3.69E-14	3.08E-14	3.22E-14
Ogasawara Islands	3.18E-14	2.65E-14	2.77E-14
Oregon, Washington, Vancouver Coast and Shelf	3.14E-14	2.62E-14	2.73E-14
Oyashio Current	4.82E-14	4.02E-14	4.19E-14
Palawan/North Borneo	2.10E-14	1.75E-14	1.83E-14
Panama Bight	2.12E-14	1.77E-14	1.85E-14
Papua	2.36E-14	1.97E-14	2.06E-14
Patagonian Shelf	3.62E-14	3.02E-14	3.15E-14
Peter the First Island	4.26E-14	3.55E-14	3.71E-14
Phoenix/Tokelau/Northern Cook Islands	2.65E-14	2.21E-14	2.30E-14
Prince Edward Islands	4.67E-14	3.89E-14	4.06E-14
Puget Trough/Georgia Basin	5.07E-14	4.23E-14	4.42E-14
Rapa-Pitcairn	3.00E-14	2.50E-14	2.61E-14
Revillagigedos	2.61E-14	2.17E-14	2.27E-14
Rio de la Plata	4.72E-16	3.94E-16	4.11E-16
Rio Grande	2.76E-14	2.31E-14	2.41E-14
Ross Sea	5.21E-14	4.35E-14	4.54E-14
Saharan Upwelling	3.13E-14	2.61E-14	2.72E-14
Sahelian Upwelling	2.92E-14	2.43E-14	2.54E-14
Samoa Islands	2.69E-14	2.24E-14	2.34E-14
Sao Pedro and Sao Paulo	2.37E-14	1.98E-14	2.06E-14

Islands			
Scotian Shelf	5.41E-14	4.51E-14	4.71E-14
Sea of Japan/East Sea	4.18E-14	3.49E-14	3.64E-14
Sea of Okhotsk	4.57E-14	3.81E-14	3.98E-14
Seychelles	2.64E-14	2.21E-14	2.30E-14
Shark Bay	2.21E-14	1.85E-14	1.93E-14
Snares Island	3.75E-14	3.13E-14	3.27E-14
Society Islands	2.08E-14	1.73E-14	1.81E-14
Solomon Archipelago	2.36E-14	1.96E-14	2.05E-14
Solomon Sea	2.40E-14	2.00E-14	2.09E-14
South and West Iceland	3.49E-14	2.91E-14	3.04E-14
South Australian Gulfs	2.87E-14	2.40E-14	2.50E-14
South China Sea Oceanic Islands	3.50E-14	2.92E-14	3.05E-14
South European Atlantic Shelf	2.84E-14	2.37E-14	2.47E-14
South Georgia	4.65E-14	3.88E-14	4.05E-14
South India and Sri Lanka	3.13E-14	2.61E-14	2.73E-14
South Kuroshio	3.32E-14	2.77E-14	2.89E-14
South New Zealand	3.57E-14	2.98E-14	3.11E-14
South Orkney Islands	5.12E-14	4.27E-14	4.46E-14
South Sandwich Islands	4.88E-14	4.07E-14	4.25E-14
South Shetland Islands	5.31E-14	4.43E-14	4.63E-14
Southeast Madagascar	2.74E-14	2.28E-14	2.38E-14
Southeast Papua New Guinea	1.70E-14	1.42E-14	1.48E-14
Southeastern Brazil	2.36E-14	1.97E-14	2.06E-14
Southern California Bight	3.35E-14	2.79E-14	2.92E-14
Southern Caribbean	2.57E-14	2.14E-14	2.24E-14
Southern China	4.04E-14	3.37E-14	3.52E-14
Southern Cook/Austral Islands	2.44E-14	2.03E-14	2.12E-14
Southern Grand Banks - South Newfoundland	5.42E-14	4.52E-14	4.72E-14
Southern Gulf of Mexico	3.10E-14	2.59E-14	2.70E-14
Southern Java	2.66E-14	2.22E-14	2.32E-14
Southern Norway	3.65E-14	3.05E-14	3.18E-14
Southern Red Sea	2.99E-14	2.50E-14	2.61E-14
Southern Vietnam	3.05E-14	2.55E-14	2.66E-14
Southwestern Caribbean	2.81E-14	2.34E-14	2.45E-14
St. Helena and Ascension Islands	3.48E-14	2.90E-14	3.03E-14
Sulawesi Sea/Makassar Strait	2.19E-14	1.83E-14	1.91E-14
Sunda Shelf/Java Sea	2.75E-14	2.30E-14	2.40E-14
Three Kings-North Cape	2.75E-14	2.30E-14	2.40E-14
Tonga Islands	2.48E-14	2.07E-14	2.16E-14
Torres Strait Northern Great Barrier Reef	2.59E-14	2.16E-14	2.25E-14
Trindade and Martin Vaz Islands	3.00E-14	2.50E-14	2.61E-14
Tristan Gough	2.92E-14	2.43E-14	2.54E-14

Tuamotus	2.56E-14	2.14E-14	2.23E-14
Tunisian Plateau/Gulf of Sidra	3.47E-14	2.90E-14	3.02E-14
Tweed-Moreton	2.76E-14	2.30E-14	2.40E-14
Uruguay-Buenos Aires Shelf	3.16E-14	2.64E-14	2.76E-14
Vanuatu	2.92E-14	2.44E-14	2.55E-14
Virginian	4.32E-14	3.60E-14	3.76E-14
Weddell Sea	4.51E-14	3.76E-14	3.93E-14
West Caroline Islands	2.69E-14	2.24E-14	2.34E-14
West Greenland Shelf	3.35E-14	2.80E-14	2.92E-14
Western and Northern Madagascar	2.37E-14	1.98E-14	2.06E-14
Western Arabian Sea	2.79E-14	2.33E-14	2.43E-14
Western Bassian	3.12E-14	2.61E-14	2.72E-14
Western Caribbean	2.02E-14	1.68E-14	1.76E-14
Western Galapagos Islands	2.84E-14	2.37E-14	2.47E-14
Western India	2.95E-14	2.46E-14	2.57E-14
Western Mediterranean	2.54E-14	2.12E-14	2.22E-14
Western Sumatra	2.34E-14	1.95E-14	2.04E-14
White Sea	2.55E-14	2.12E-14	2.22E-14
Yellow Sea	4.52E-14	3.77E-14	3.94E-14

*Table S7: Midpoint characterization factor values for CO_2, CH_4, and CO [pH*yr/kg] per FAO major fishing area*

FAO major fishing area	CO_2	CH_4	CO
18	4.78E-14	3.99E-14	4.16E-14
21	1.52E-14	1.27E-14	1.33E-14
27	2.70E-14	2.25E-14	2.35E-14
31	2.60E-14	2.17E-14	2.27E-14
34	2.17E-14	1.81E-14	1.89E-14
41	3.04E-14	2.53E-14	2.65E-14
47	3.05E-14	2.54E-14	2.66E-14
48	2.68E-14	2.23E-14	2.33E-14
51	3.48E-14	2.90E-14	3.03E-14
57	3.39E-14	2.83E-14	2.95E-14
58	3.61E-14	3.01E-14	3.15E-14
61	3.52E-14	2.94E-14	3.07E-14
67	2.47E-14	2.06E-14	2.15E-14
71	2.24E-14	1.87E-14	1.95E-14
77	2.38E-14	1.99E-14	2.07E-14
81	3.89E-14	3.25E-14	3.39E-14
87	2.94E-14	2.45E-14	2.56E-14
88	2.12E-14	1.76E-14	1.84E-14

Figure S1: Data variability within MERs vs FAOs of spCO2 and pH

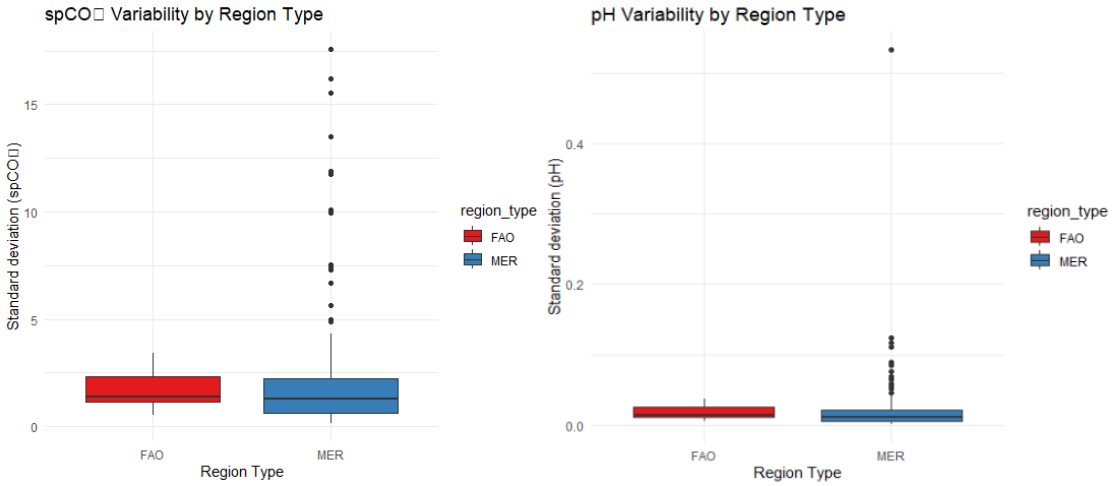

Though the FAO regions are larger than the MERs, with our data we are only looking at the top layer of ocean, which, for open ocean, is relatively homogenous. The coastal marine ecoregions, though often smaller, are more heterogenous than open ocean regions. Though there are data outliers, we chose to use averages rather than medians because the median would underrepresent the more common values within each marine ecoregion when such outliers are present. In this context, the average provides a more representative estimate of the general conditions and therefore a more appropriate basis for calculating characterization factors.

Figure S2: HC50 and HC20$_{pH10}$ SSD curves for strongly calcifying species

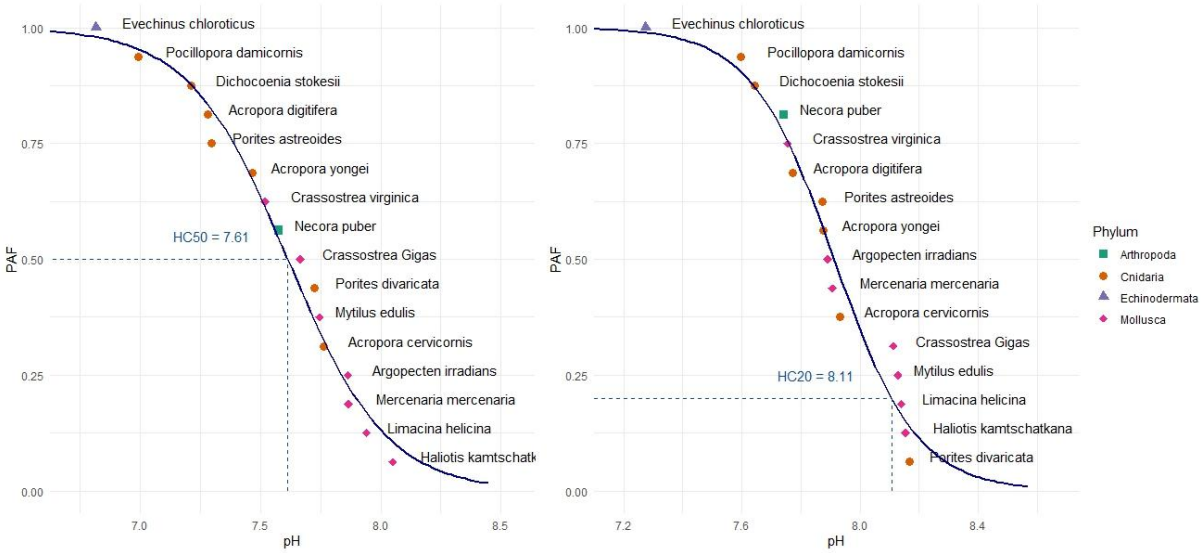

Figure S3: HC50 and HC20$_{pH10}$ SSD curves for slightly calcifying species

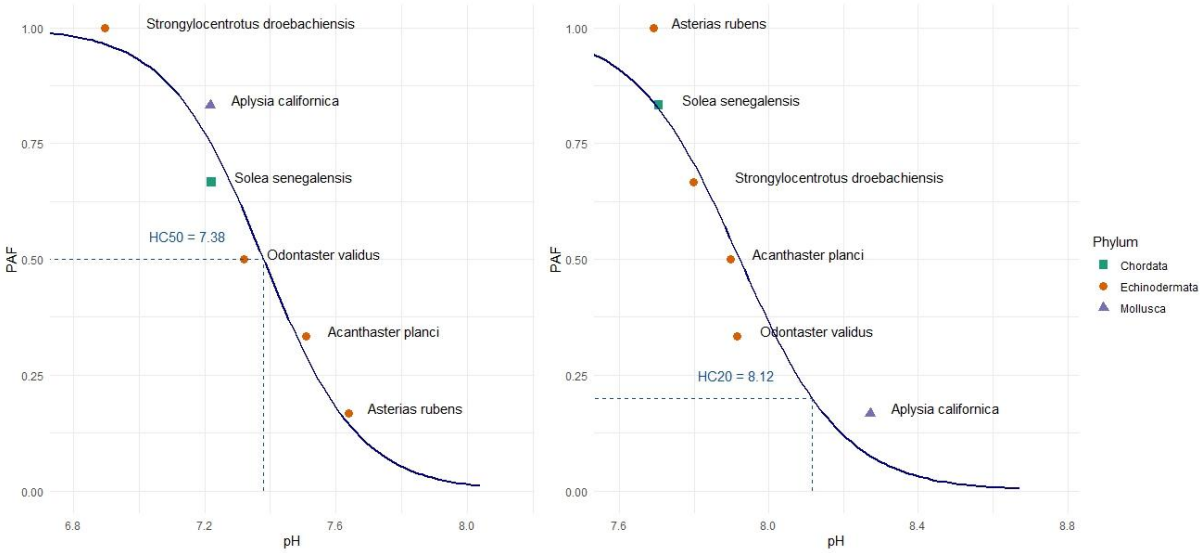

Figure S4: SSD curves for non-calcifying species

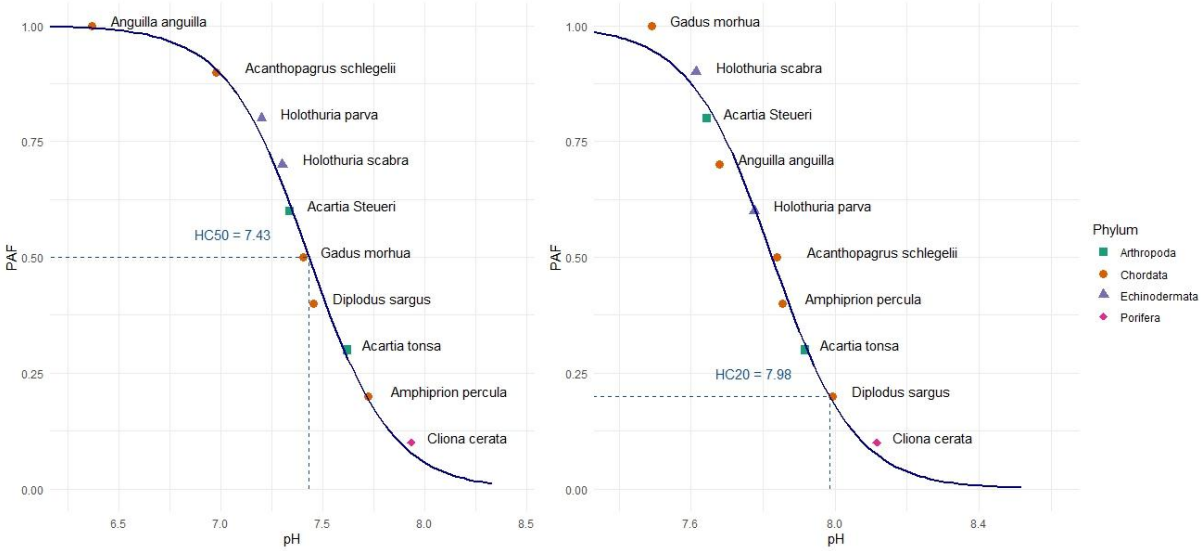

Figure S5: HC50 and HC20$_{pH10}$ SSD curves for tropical species

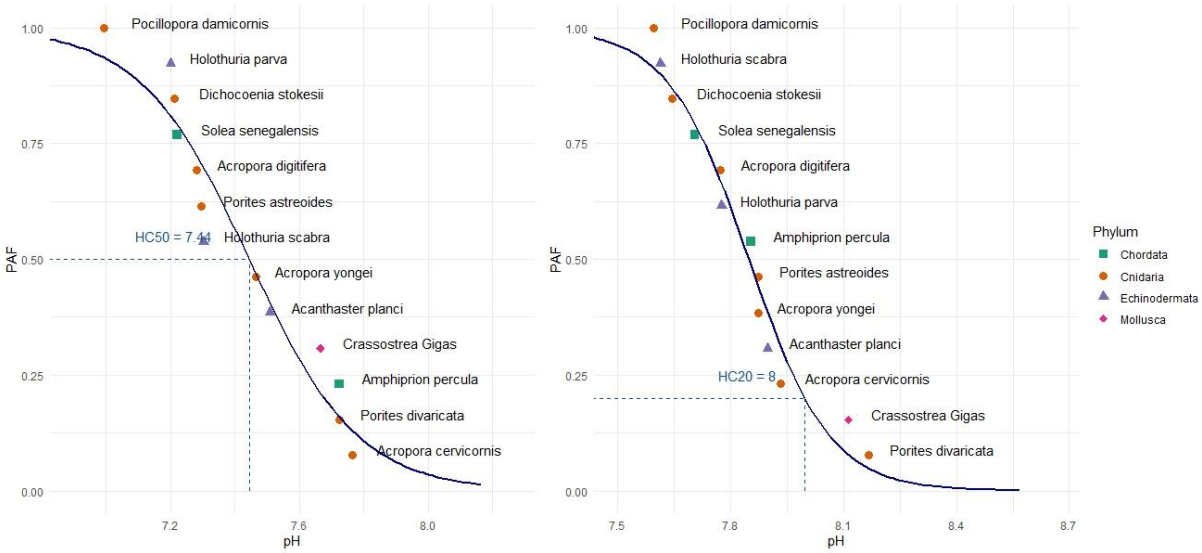

Figure S6: HC50 and HC20$_{pH10}$ SSD curves for subtropical species

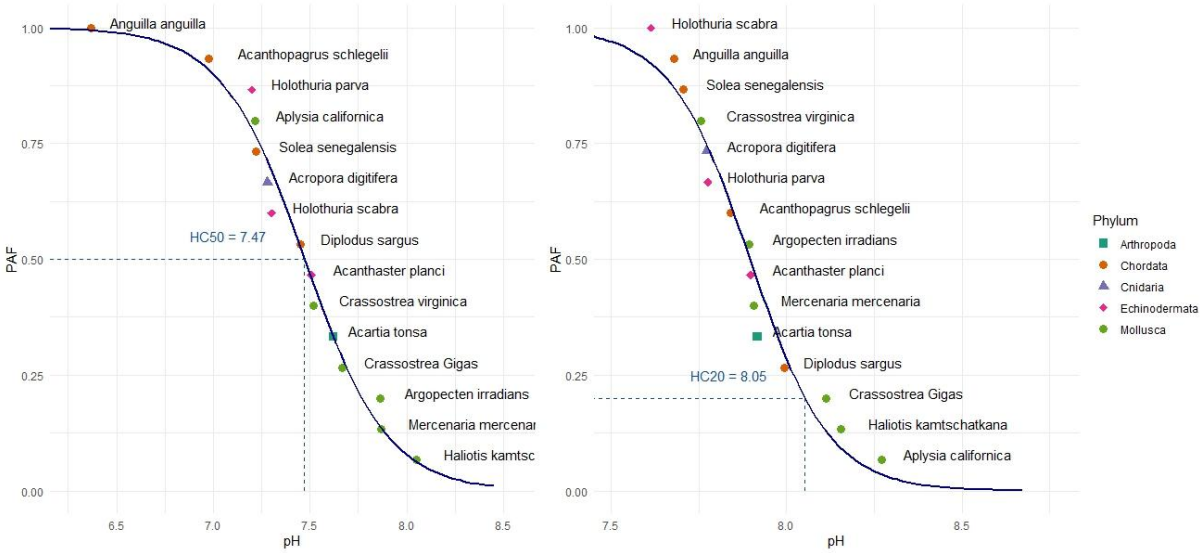

Figure S7: HC50 and HC20$_{pH10}$ SSD curves for temperate species

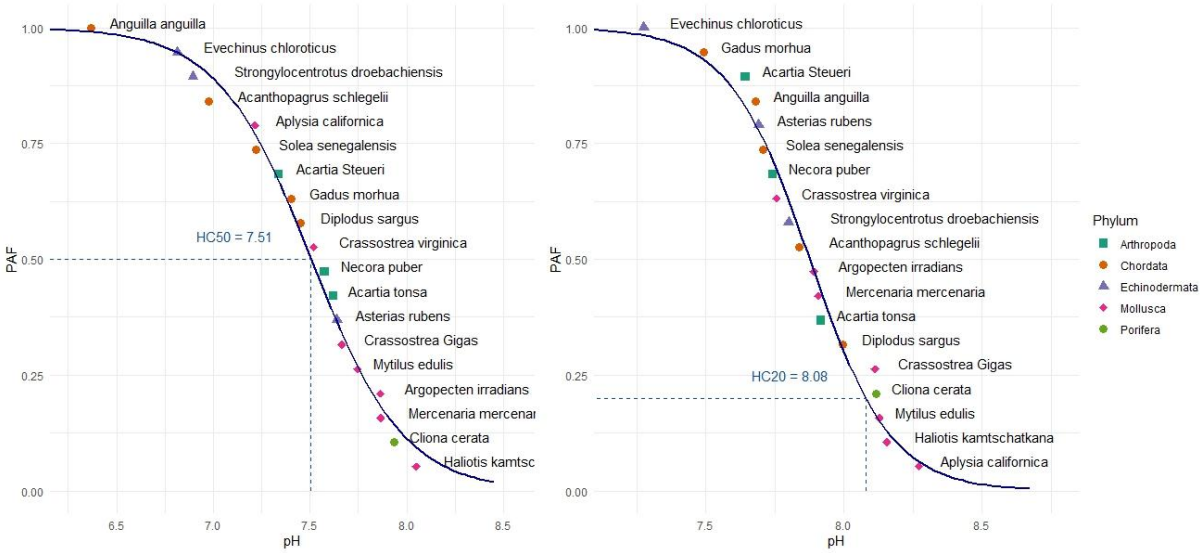

Figure S8: HC50 and HC20$_{pH10}$ SSD curves for polar species

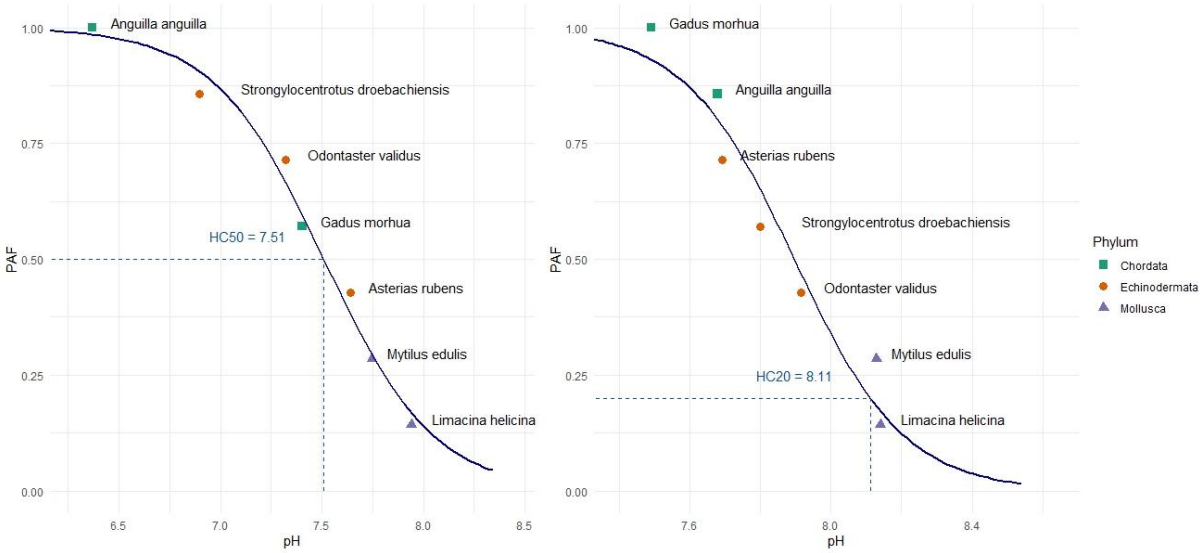

*Table S8: Endpoint characterization factor values for CO_2, CH_4, and CO [PDF*yr/kg] per marine*

ecoregion

Marine ecoregion	CO_2	CH_4	CO
Adriatic Sea	4.72E-14	3.94E-14	4.11E-14
Aegean Sea	6.21E-14	5.18E-14	5.41E-14
Agulhas Bank	3.97E-14	3.31E-14	3.45E-14
Alboran Sea	4.49E-14	3.74E-14	3.91E-14
Aleutian Islands	5.77E-14	4.81E-14	5.03E-14
Amazonia	4.53E-14	3.78E-14	3.95E-14
Amsterdam-St Paul	3.79E-14	3.16E-14	3.30E-14
Amundsen/Bellingshausen Sea	6.91E-14	5.77E-14	6.02E-14
Andaman and Nicobar Islands	4.10E-14	3.42E-14	3.57E-14
Andaman Sea Coral Coast	3.68E-14	3.07E-14	3.21E-14
Angolan	3.41E-14	2.84E-14	2.97E-14
Antarctic Peninsula	6.90E-14	5.76E-14	6.01E-14
Arabian (Persian) Gulf	4.55E-14	3.80E-14	3.96E-14
Arafura Sea	2.24E-14	1.87E-14	1.95E-14
Araucanian	4.54E-14	3.79E-14	3.95E-14
Arnhem Coast to Gulf of Carpenteria	2.92E-14	2.44E-14	2.54E-14
Auckland Island	5.32E-14	4.43E-14	4.63E-14
Azores Canaries Madeira	3.59E-14	2.99E-14	3.13E-14
Baffin Bay - Davis Strait	6.18E-14	5.16E-14	5.38E-14
Bahamian	5.01E-14	4.18E-14	4.37E-14
Baltic Sea	6.87E-14	5.73E-14	5.98E-14
Banda Sea	3.61E-14	3.01E-14	3.15E-14
Bassian	4.51E-14	3.77E-14	3.93E-14
Beaufort Sea - continental coast and shelf	4.96E-14	4.13E-14	4.32E-14
Beaufort-Amundsen-Viscount Melville-Queen Maud	7.72E-14	6.44E-14	6.72E-14
Bermuda	4.23E-14	3.53E-14	3.68E-14
Bight of Sofala/Swamp Coast	2.13E-14	1.78E-14	1.86E-14
Bismarck Sea	3.03E-14	2.52E-14	2.63E-14
Black Sea	3.39E-14	2.83E-14	2.96E-14
Bonaparte Coast	2.10E-14	1.75E-14	1.83E-14
Bounty and Antipodes Islands	5.26E-14	4.39E-14	4.59E-14
Bouvet Island	6.60E-14	5.50E-14	5.75E-14
Campbell Island	5.68E-14	4.74E-14	4.95E-14
Cape Howe	3.86E-14	3.22E-14	3.36E-14
Cape Verde	3.76E-14	3.13E-14	3.27E-14
Cargados Carajos/Tromelin Island	3.96E-14	3.31E-14	3.45E-14
Carolinian	4.70E-14	3.92E-14	4.10E-14
Celtic Seas	4.37E-14	3.64E-14	3.80E-14
Central and Southern Great Barrier Reef	2.83E-14	2.36E-14	2.47E-14
Central Chile	3.87E-14	3.23E-14	3.37E-14
Central Kuroshio Current	4.64E-14	3.87E-14	4.04E-14

Central New Zealand	4.28E-14	3.57E-14	3.73E-14
Central Peru	4.35E-14	3.63E-14	3.79E-14
Central Somali Coast	4.03E-14	3.36E-14	3.51E-14
Chagos	2.78E-14	2.32E-14	2.43E-14
Channels and Fjords of Southern Chile	5.14E-14	4.29E-14	4.48E-14
Chatham Island	4.42E-14	3.69E-14	3.85E-14
Chiapas-Nicaragua	3.37E-14	2.81E-14	2.94E-14
Chiloense	5.08E-14	4.24E-14	4.43E-14
Chukchi Sea	6.22E-14	5.19E-14	5.42E-14
Clipperton	3.61E-14	3.01E-14	3.14E-14
Cocos Islands	3.25E-14	2.71E-14	2.83E-14
Cocos-Keeling/Christmas Island	3.23E-14	2.70E-14	2.82E-14
Coral Sea	4.05E-14	3.38E-14	3.53E-14
Cortezian	4.33E-14	3.62E-14	3.78E-14
Crozet Islands	5.24E-14	4.37E-14	4.57E-14
Delagoa	2.99E-14	2.49E-14	2.60E-14
East African Coral Coast	2.40E-14	2.00E-14	2.09E-14
East Antarctic Dronning Maud Land	6.70E-14	5.59E-14	5.83E-14
East Antarctic Enderby Land	7.62E-14	6.36E-14	6.64E-14
East Antarctic Wilkes Land	6.76E-14	5.64E-14	5.89E-14
East Caroline Islands	3.51E-14	2.92E-14	3.05E-14
East China Sea	3.58E-14	2.98E-14	3.12E-14
East Greenland Shelf	4.89E-14	4.08E-14	4.26E-14
East Siberian Sea	9.35E-14	7.80E-14	8.14E-14
Easter Island	4.48E-14	3.73E-14	3.90E-14
Eastern Bering Sea	5.29E-14	4.42E-14	4.61E-14
Eastern Brazil	3.28E-14	2.74E-14	2.86E-14
Eastern Caribbean	4.99E-14	4.16E-14	4.35E-14
Eastern Galapagos Islands	3.41E-14	2.85E-14	2.97E-14
Eastern India	4.96E-14	4.13E-14	4.32E-14
Eastern Philippines	3.01E-14	2.51E-14	2.63E-14
Exmouth to Broome	2.69E-14	2.25E-14	2.35E-14
Faroe Plateau	4.16E-14	3.47E-14	3.63E-14
Fernando de Naronha and Atoll das Rocas	3.88E-14	3.23E-14	3.38E-14
Fiji Islands	4.75E-14	3.96E-14	4.14E-14
Floridian	4.92E-14	4.10E-14	4.28E-14
Gilbert/Ellis Islands	3.41E-14	2.84E-14	2.97E-14
Great Australian Bight	3.82E-14	3.18E-14	3.33E-14
Greater Antilles	4.33E-14	3.61E-14	3.77E-14
Guayaquil	4.09E-14	3.41E-14	3.56E-14
Guianan	2.42E-14	2.02E-14	2.11E-14
Gulf of Aden	4.07E-14	3.40E-14	3.55E-14
Gulf of Alaska	5.31E-14	4.43E-14	4.63E-14

Gulf of Guinea Central	2.98E-14	2.48E-14	2.59E-14
Gulf of Guinea Islands	2.98E-14	2.48E-14	2.59E-14
Gulf of Guinea South	3.14E-14	2.62E-14	2.74E-14
Gulf of Guinea Upwelling	3.67E-14	3.06E-14	3.20E-14
Gulf of Guinea West	3.22E-14	2.69E-14	2.81E-14
Gulf of Maine/Bay of Fundy	7.27E-14	6.07E-14	6.33E-14
Gulf of Oman	3.78E-14	3.15E-14	3.29E-14
Gulf of Papua	2.47E-14	2.06E-14	2.15E-14
Gulf of St. Lawrence - Eastern Scotian Shelf	7.67E-14	6.39E-14	6.68E-14
Gulf of Thailand	2.13E-14	1.77E-14	1.85E-14
Gulf of Tonkin	5.23E-14	4.36E-14	4.56E-14
Halmahera	3.40E-14	2.84E-14	2.96E-14
Hawaii	4.36E-14	3.64E-14	3.80E-14
Heard and Macdonald Islands	7.05E-14	5.88E-14	6.14E-14
High Arctic Archipelago	7.13E-14	5.95E-14	6.21E-14
Houtman	3.86E-14	3.22E-14	3.36E-14
Hudson Complex	3.88E-14	3.24E-14	3.38E-14
Humboldtian	3.99E-14	3.33E-14	3.47E-14
Ionian Sea	4.14E-14	3.46E-14	3.61E-14
Juan Fernandez and Desventuradas	3.98E-14	3.32E-14	3.46E-14
Kamchatka Shelf and Coast	5.60E-14	4.67E-14	4.88E-14
Kara Sea	5.82E-14	4.85E-14	5.07E-14
Kerguelen Islands	6.14E-14	5.13E-14	5.35E-14
Kermadec Island	3.18E-14	2.65E-14	2.77E-14
Lancaster Sound	7.32E-14	6.10E-14	6.37E-14
Laptev Sea	1.23E-13	1.03E-13	1.07E-13
Leeuwin	4.28E-14	3.57E-14	3.73E-14
Lesser Sunda	3.66E-14	3.06E-14	3.19E-14
Levantine Sea	3.81E-14	3.18E-14	3.32E-14
Line Islands	3.66E-14	3.05E-14	3.18E-14
Lord Howe and Norfolk Islands	3.21E-14	2.68E-14	2.80E-14
Macquarie Island	4.54E-14	3.79E-14	3.95E-14
Magdalena Transition	4.42E-14	3.69E-14	3.85E-14
Malacca Strait	2.60E-14	2.17E-14	2.27E-14
Maldives	3.79E-14	3.16E-14	3.30E-14
Malvinas/Falklands	5.25E-14	4.38E-14	4.57E-14
Manning-Hawkesbury	3.60E-14	3.00E-14	3.13E-14
Mariana Islands	4.21E-14	3.51E-14	3.67E-14
Marquesas	3.88E-14	3.24E-14	3.38E-14
Marshall Islands	3.65E-14	3.04E-14	3.18E-14
Mascarene Islands	3.64E-14	3.04E-14	3.17E-14
Mexican Tropical Pacific	3.73E-14	3.11E-14	3.25E-14
Namaqua	3.87E-14	3.23E-14	3.37E-14
Namib	3.97E-14	3.31E-14	3.46E-14
Natal	3.77E-14	3.14E-14	3.28E-14

New Caledonia	3.38E-14	2.82E-14	2.94E-14
Nicoya	3.29E-14	2.74E-14	2.86E-14
Ningaloo	4.30E-14	3.59E-14	3.75E-14
North American Pacific Fijordland	4.98E-14	4.16E-14	4.34E-14
North and East Barents Sea	4.43E-14	3.69E-14	3.86E-14
North and East Iceland	4.85E-14	4.05E-14	4.23E-14
North Greenland	6.27E-14	5.23E-14	5.46E-14
North Patagonian Gulfs	4.66E-14	3.89E-14	4.06E-14
North Sea	7.02E-14	5.86E-14	6.12E-14
Northeast Sulawesi	3.43E-14	2.86E-14	2.98E-14
Northeastern Brazil	4.45E-14	3.71E-14	3.87E-14
Northeastern Honshu	4.82E-14	4.02E-14	4.20E-14
Northeastern New Zealand	3.87E-14	3.23E-14	3.37E-14
Northern and Central Red Sea	4.35E-14	3.63E-14	3.79E-14
Northern Bay of Bengal	5.44E-14	4.54E-14	4.74E-14
Northern California	4.39E-14	3.66E-14	3.82E-14
Northern Galapagos Islands	3.55E-14	2.96E-14	3.09E-14
Northern Grand Banks - Southern Labrador	5.08E-14	4.24E-14	4.42E-14
Northern Gulf of Mexico	4.70E-14	3.92E-14	4.09E-14
Northern Labrador	6.32E-14	5.27E-14	5.51E-14
Northern Monsoon Current Coast	3.70E-14	3.09E-14	3.22E-14
Northern Norway and Finnmark	4.97E-14	4.15E-14	4.33E-14
Ogasawara Islands	4.28E-14	3.57E-14	3.73E-14
Oregon, Washington, Vancouver Coast and Shelf	4.23E-14	3.53E-14	3.68E-14
Oyashio Current	6.49E-14	5.41E-14	5.65E-14
Palawan/North Borneo	2.83E-14	2.36E-14	2.46E-14
Panama Bight	2.86E-14	2.38E-14	2.49E-14
Papua	3.18E-14	2.65E-14	2.77E-14
Patagonian Shelf	4.87E-14	4.06E-14	4.24E-14
Peter the First Island	5.74E-14	4.79E-14	5.00E-14
Phoenix/Tokelau/Northern Cook Islands	3.56E-14	2.97E-14	3.10E-14
Prince Edward Islands	6.28E-14	5.24E-14	5.47E-14
Puget Trough/Georgia Basin	6.83E-14	5.70E-14	5.95E-14
Rapa-Pitcairn	4.04E-14	3.37E-14	3.51E-14
Revillagigedos	3.51E-14	2.93E-14	3.06E-14
Rio de la Plata	6.36E-16	5.30E-16	5.54E-16
Rio Grande	3.72E-14	3.11E-14	3.24E-14
Ross Sea	7.02E-14	5.86E-14	6.12E-14
Saharan Upwelling	4.21E-14	3.51E-14	3.67E-14
Sahelian Upwelling	3.93E-14	3.28E-14	3.42E-14
Samoa Islands	3.62E-14	3.02E-14	3.15E-14
Sao Pedro and Sao Paulo Islands	3.19E-14	2.66E-14	2.78E-14

Scotian Shelf	7.29E-14	6.08E-14	6.35E-14
Sea of Japan/East Sea	5.64E-14	4.70E-14	4.91E-14
Sea of Okhotsk	6.15E-14	5.13E-14	5.36E-14
Seychelles	3.56E-14	2.97E-14	3.10E-14
Shark Bay	2.98E-14	2.49E-14	2.60E-14
Snares Island	5.05E-14	4.22E-14	4.40E-14
Society Islands	2.80E-14	2.33E-14	2.44E-14
Solomon Archipelago	3.17E-14	2.65E-14	2.76E-14
Solomon Sea	3.23E-14	2.70E-14	2.82E-14
South and West Iceland	4.70E-14	3.92E-14	4.09E-14
South Australian Gulfs	3.87E-14	3.23E-14	3.37E-14
South China Sea Oceanic Islands	4.72E-14	3.94E-14	4.11E-14
South European Atlantic Shelf	3.83E-14	3.19E-14	3.33E-14
South Georgia	6.26E-14	5.22E-14	5.45E-14
South India and Sri Lanka	4.22E-14	3.52E-14	3.67E-14
South Kuroshio	4.48E-14	3.73E-14	3.90E-14
South New Zealand	4.80E-14	4.01E-14	4.18E-14
South Orkney Islands	6.89E-14	5.75E-14	6.00E-14
South Sandwich Islands	6.57E-14	5.48E-14	5.72E-14
South Shetland Islands	7.16E-14	5.97E-14	6.24E-14
Southeast Madagascar	3.69E-14	3.08E-14	3.21E-14
Southeast Papua New Guinea	2.29E-14	1.91E-14	1.99E-14
Southeastern Brazil	3.18E-14	2.65E-14	2.77E-14
Southern California Bight	4.51E-14	3.76E-14	3.93E-14
Southern Caribbean	3.46E-14	2.89E-14	3.02E-14
Southern China	5.44E-14	4.54E-14	4.74E-14
Southern Cook/Austral Islands	3.28E-14	2.74E-14	2.86E-14
Southern Grand Banks - South Newfoundland	7.30E-14	6.09E-14	6.36E-14
Southern Gulf of Mexico	4.18E-14	3.48E-14	3.64E-14
Southern Java	3.59E-14	2.99E-14	3.13E-14
Southern Norway	4.92E-14	4.11E-14	4.29E-14
Southern Red Sea	4.03E-14	3.36E-14	3.51E-14
Southern Vietnam	4.11E-14	3.43E-14	3.58E-14
Southwestern Caribbean	3.78E-14	3.16E-14	3.30E-14
St. Helena and Ascension Islands	4.68E-14	3.91E-14	4.08E-14
Sulawesi Sea/Makassar Strait	2.95E-14	2.46E-14	2.57E-14
Sunda Shelf/Java Sea	3.71E-14	3.09E-14	3.23E-14
Three Kings-North Cape	3.71E-14	3.09E-14	3.23E-14
Tonga Islands	3.35E-14	2.79E-14	2.91E-14
Torres Strait Northern Great Barrier Reef	3.48E-14	2.91E-14	3.03E-14
Trindade and Martin Vaz Islands	4.04E-14	3.37E-14	3.51E-14
Tristan Gough	3.93E-14	3.28E-14	3.42E-14
Tuamotus	3.45E-14	2.88E-14	3.01E-14

Tunisian Plateau/Gulf of Sidra	4.68E-14	3.90E-14	4.07E-14
Tweed-Moreton	3.71E-14	3.10E-14	3.23E-14
Uruguay-Buenos Aires Shelf	4.26E-14	3.55E-14	3.71E-14
Vanuatu	3.94E-14	3.28E-14	3.43E-14
Virginian	5.82E-14	4.85E-14	5.07E-14
Weddell Sea	6.08E-14	5.07E-14	5.29E-14
West Caroline Islands	3.62E-14	3.02E-14	3.15E-14
West Greenland Shelf	4.52E-14	3.77E-14	3.93E-14
Western and Northern Madagascar	3.19E-14	2.66E-14	2.78E-14
Western Arabian Sea	3.76E-14	3.14E-14	3.28E-14
Western Bassian	4.21E-14	3.51E-14	3.67E-14
Western Caribbean	2.72E-14	2.27E-14	2.37E-14
Western Galapagos Islands	3.82E-14	3.19E-14	3.33E-14
Western India	3.97E-14	3.31E-14	3.46E-14
Western Mediterranean	3.43E-14	2.86E-14	2.98E-14
Western Sumatra	3.16E-14	2.63E-14	2.75E-14
White Sea	3.43E-14	2.86E-14	2.99E-14
Yellow Sea	6.09E-14	5.08E-14	5.30E-14

*Table S9: Endpoint characterization factor values for CO_2, CH_4, and CO [PDF*yr/kg] per FAO major fishing areas*

FAO major fishing area	**CO_2**	**CH_4**	**CO**
18	6.44E-14	5.37E-14	5.61E-14
21	2.05E-14	1.71E-14	1.79E-14
27	3.64E-14	3.04E-14	3.17E-14
31	3.51E-14	2.93E-14	3.06E-14
34	2.93E-14	2.44E-14	2.55E-14
41	4.09E-14	3.41E-14	3.56E-14
47	4.11E-14	3.43E-14	3.58E-14
48	3.60E-14	3.01E-14	3.14E-14
51	4.69E-14	3.91E-14	4.08E-14
57	4.57E-14	3.81E-14	3.98E-14
58	4.87E-14	4.06E-14	4.24E-14
61	4.74E-14	3.95E-14	4.13E-14
67	3.32E-14	2.77E-14	2.90E-14
71	3.02E-14	2.52E-14	2.63E-14
77	3.21E-14	2.68E-14	2.79E-14
81	5.24E-14	4.37E-14	4.57E-14
87	3.95E-14	3.30E-14	3.44E-14
88	2.85E-14	2.38E-14	2.48E-14